The Edge Flaking of Tungsten Carbide Hardmetal Cermets under Repetitive Impact Loading

By

Deon du Randt

A thesis submitted to the Faculty of Engineering, University of Cape Town, for the degree of Master of Science in Engineering

Department of Materials Engineering

University of Cape Town

November 1995

Contents

Table of Figures

Abstract

Repetitive impact tests were carried out in order to determine the edge flaking performance of several grades of hardmetal cermets. In an attempt to understand the geometry and characteristics of the crack propagation glass was impacted. Various types of cracking are observed in the glass including crushing, lateral cracking, median cracking and Hertzian cone cracking. The results of the glass impacting were then compared with those observed in the hardmetal cermets. Hertzian cone cracking dominates in the cermets. The fractography of the crack surfaces and crack paths, occurring in the cermets, have been studied in order to explain the edge flaking performance. Contiguity and mean-free path are found to have important influences on the edge flaking performance. The performances of the various grades of hardmetal cermets are compared in an attempt to rank them in relation to their susceptibility to edge flake.

Introduction

Tungsten carbide cermets (WC-cermets) are a product of a mature technology. Tungsten carbide cobalt hardmetals emerged after Schroter's invention in 1923. They were first used in production shortly after that in 1926 for dies for the hot drawing of tungsten wire [Tracey, 1992]. Since then WC-cermets have become widely used in various engineering applications where high wear resistance and impact properties are necessary. These two properties are as result of its composite structure. The wear resistance comes primarily from the hard carbide particles while the toughness is attributable to the metallic binder phase.

WC hardmetals have been in existence for many years and are today still widely used. This cermet has therefore have been widely researched and many aspects of it have received much attention especially of late. It appears that even with all the research that has been done there are still many areas where more specialised testing has to be done to clarify what occurs in practice. Roebuck and Almond (1988) stated that in the past not enough was understood about the crack topology and the chemistry of crack paths. An appreciable amount of work has been done on the general wear of WC-cermets especially in erosion, fatigue and static fracture testing.

Fatigue testing involves high cycle fracture by means of slow crack growth while in static fracture testing the crack growth is as a result of fast fracture brought about by a single loading of the test piece. In order to study this fast fracture in a manner that imitates what occurs in practice more closely, a repetitive impact technique has been used. The testing involves the edge flaking of various grades of WC-cermet under repetitive impact. Edge flaking is an important cause of damage in brittle tool materials and can be a major life limiting factor [Mc Cormick, 1992].

The objectives of this investigation were therefore:

i) To evaluate edge flake resistance of a range of cobalt binder, nickel-chromium binder and nickel-chromium-cobalt binder WC-cermets under repetitive impact. The influence of the microstructure of these cermets on their edge flake resistance is discussed.

ii) To perform a microscopy study to characterise the crack modes and crack topography in these cermets. This study includes optical and scanning electron work.

iii) To understand the mechanistics of the crack growth modes in these cermets and thus the shape of the flake that forms was modelled by the impacting of glass.

Structure and Chemical Composition of WC-Cermets

Tungsten carbide phase

Exner (1979) states that it is well established that tungsten forms two hexagonal carbides; the monocarbide WC and the subcarbide W_2C. Doeg (1960), Luyckx (1970) and Exner (1979) report that the dimensions of the monocarbide are a = 2.906Å, c = 2.837Å and c/a = 0.975 which corresponds to a density of 15.77 g/cm^3. The WC phase has a hardness of 2400-2500 VPN. The W_2C phase has lattice parameters of a = 2.98Å and c = 4.71Å which corresponds to a density of 17.34 g/cm$_3$. The W_2C phase is a high temperature intermediate phase. Exner (1979) states that 98% of all hardmetal grades contain WC. Doeg (1960) explains that a deficiency in carbon levels leads to the formation of the brittle eta phase (W_3Co_3C) and an excess leads to free carbon.

Binder Phase

The two binder phases that are of importance in this study are pure cobalt and nickel with alloying additions of cobalt and chromium.

Doeg (1960) explains that cobalt is a very good metal to use as the binder phase for two reasons. Firstly, as it has a low tendency to form carbides and, secondly, it has a low angle of contact with WC and thus wets the WC grains well. The bonding strength of a metal to carbide decreases with an increasing tendency for carbide stability.

As stated by Tracey (1992) the lattice parameter of nickel (0.352nm) is only slightly less than face centred cubic (fcc) cobalt (0.354nm). The main differences are that the fcc cobalt is metastable and can transform to a

hexagonally close packed (hcp) structure and that cobalt is substantially more magnetic.

Ekemar, Lindholm and Hartzell (1982) reports that WC-Co grades with nickel and chromium additions show an improved corrosion and oxidation resistance and are not as susceptible as plain WC-Co to thermal cracking. These improvements have been attained at the expense of transverse rupture strength (TRS) with a strength reduction of about 20%.

Cooper, Manktelow and Wong (1988) states that the substitution of a Ni-Cr binder for cobalt improves the corrosion resistance and chromium carbide inhibits grain growth. They go further to say that in both cases chromium has been associated with excessive porosity and reduced toughness in the sintered product.

Microstructural Parameters of Cemented Carbide

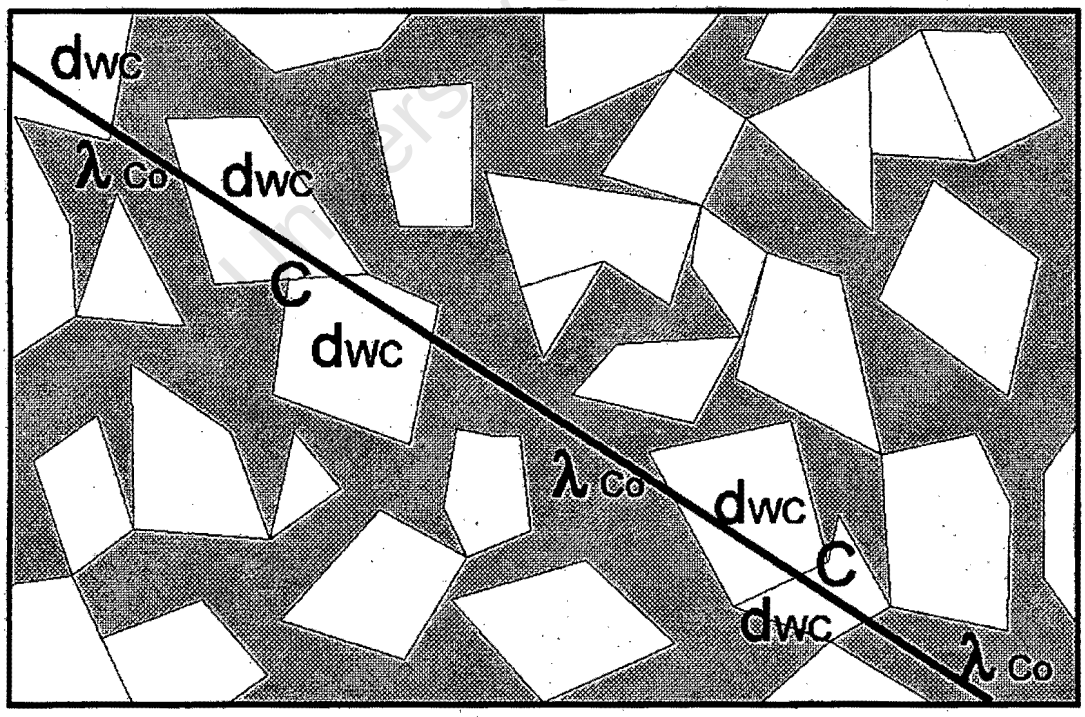

Figure 1. Schematic of microstructural parameters of WC-cermet

Where λ_{Co} = mean-free path of binder phase

d_{WC} = Tungsten carbide grain size

C = contiguity

The mean-free path of the binder is the average length of the segments of the line that intersects this binder. Lee and Gurland (1978) state that the contiguity is the fraction of the total internal surface area of a phase that is shared by particles of the same phase. For WC-cermets the contiguity is a measure of the amount of contact of the WC grains.

Contiguity

Luyckx (1968) reports that most authors agree WC-Co cermets consist of a continuous WC skeleton up to cobalt contents of 10-15% and above that this skeleton becomes discontinuous. Lee and Gurland (1978) state that the existence of a continuous carbide skeleton is very probable in high carbide alloys and that the larger the WC particle size the greater the contiguity. Exner and Gurland (1970) concluded that a modified skeleton theory was more widely accepted. They continue to explain that contiguity varies with cobalt content, sintering time and sintering temperature. Exner (1979) states that an increased cobalt content caused a gradually decreasing contiguity and that this continued until around 20% cobalt by volume.

Friederich (1983) concluded that in a WC-cermet with 12 wt % cobalt binder this binder does not form a continuous film between all the WC grains. While Sharma, Ward, Fraser and Williams (1980) state that cobalt is always present as a film, in a 6% WC binder cermet, between the grains. Laugier (1985 a) after studying WC powder before sintering reported that some aggregates of tungsten consist of crystallographicaly well aligned WC grains which should be very stable even during sintering and this would mean that no cobalt would penetrate between these aligned grains.

Hardness

WC-cermets obtain their high hardness from the hard brittle carbide phase. The binder phase is considered to be continuous, but there is apparently disagreement about the degree of contiguity of the carbide phase. Lee and Gurland (1978) refer to electron microscopic studies that record deformation by slip in the WC particles which is given as a reason for bulk deformation of the cermet to occur where there is a continuous carbide skeleton. Another school of thought assumes carbide particles are embedded in a continuous binder phase with thin cobalt films separating the individual carbide grains. For this model binder phase will play a dominant role in the plastic deformation of WC-cermets.

Laugier (1985 b) states that, for WC-Co composites containing up to about 50% cobalt by volume, the hardness is controlled by the cobalt phase. He explains this in terms of the clustering of the WC phase. It is assumed that the WC grains, which are in apparent contact, are generally separated by a thin layer of cobalt. There is thus no contiguity in the true sense of the word. This phenomenon can be viewed as a measure of WC clustering tendency. The mechanical properties of the cobalt phase and the plastic constraint on the cobalt phase, due to apparent contiguity, thus govern the hardness of WC-Co cermets.

Fracture Toughness

Fracture toughness is just one of the methods used to estimate a materials ability to withstand fracture. Fracture toughness (K_{IC}) is a material property and in the plane strain condition K_{IC} is defined as:

$$K_{IC} = \sigma.\gamma \sqrt{\pi.a}$$

where σ =critical tensile stress

γ = geometry factor

a = crack length

The fracture toughness of a WC-cermet is increased with increasing binder percentage and increasing grain size. Both increased binder percentage and increased grain size increase the mean-free path of the binder. With a higher mean-free path of the binder the cracks that grow in the cermet undergo a higher amount of plastic deformation and this absorbs more energy thus improving their fracture toughness. The binder is also under less plastic constraint with a higher mean free path and will therefore behave in a more ductile manner.

Thermal Stresses

Exner and Gurland (1970) state that considerable stresses arise in WC-Co during cooling from sintering temperatures. This arises from the fact that cobalt has a thermal expansion coefficient of about three times that of WC grains. Gurland (1958) and Bernard (1963) measured tensile stresses in the WC phase in low cobalt compositions, however, using a more refined analytical technique other researchers have concluded that there are compressive stresses in the WC grains in all compositions [Öhman, Pärnama and Palmqvist (1967); Palmqvist (1963); French (1969)]. Exner and Gurland (1970) report that some researchers believe these internal stresses to be of importance while other researchers do not.

Types of Failure that occur in Rock Drilling

Methods of Drilling

Three main types of drilling are employed for rock cutting. These include rotary, percussive and rotary-percussive drilling. It is stated by Luyckx (1986) that rotary drilling is used with rocks of a compressive strength of < 280 N/mm^2. For harder rocks with a higher compressive strength percussive drilling is used. Larsen-Basse (1983) states that the wear of the tool bit is a major factor in determining the energy requirements and the penetration rate in rock drilling, and it often dictates the choice of drilling method for a certain type of rock.

Rotary Drilling

Of these three types of drilling rotary drilling involves the least amount of impact and the most abrasion. The high degree of abrasion is due to the WC-cermet inserts being dragged across the rock face. Larsen-Basse (1983) explains that bit life can be increased by increasing insert hardness up to the level at which brittle fracture begins to dominate.

Percussive Drilling

Larsen-Basse (1973) states that percussive drilling is relatively inefficient, resulting in only 60-70% of the energy being transmitted to the rock, this is because the rock is broken into excessively small fragments and the time of actual material removal is only a small fraction of the total drill time. Both Larsen-Basse (1973) and Luyckx (1986) agree that this type of drilling is necessary to drill very hard rocks.

Larsen-Basse (1983) states that the bits used for this type of drilling are susceptible to brittle impact spalling, fatigue and abrasion from rock particles. Drilling in hard rock causes material to be lost, from the hardmetal inserts, by

flaking or chipping while for softer and more abrasive rock abrasion is the dominant cause of material removal.

Rotary-Percussive Drilling

Rotary-percussive drilling is more widely used than percussive drilling and is carried out by cylindrical bits which have hemispherical or conical carbide button inserts. Larsen-Basse (1983) reports that material is removed from the rock face by crushing and the formation of cracks during the impact contact. This facilitates the removal of rock during the part of the cycle that cutting occurs. The cutting occurs when the bit is in contact with the rock face. The tool bit remains under compression most of the time which can improve its life. If a compressive stress is not maintained fatigue may substantially reduce the life of the bit. The bit is subjected to lower compressive stresses and even tensile stresses if it is under thrusted during drilling. Under thrusting can occur due to the rock drill not having enough power or the rock drill operator not allowing enough force to be applied to the drill. The wear, to the carbide inserts, occurs by abrasion, brittle fracture and impact-fatigue in this type of drilling according to Larsen-Basse (1983).

Influence of Microstructure on Rotary- Percussive Tool Insert Fracture

Hack and Peters (1985) detailed the fracture types that occur during the drilling of hard rock. They state that one of the important properties controlling this wear is fracture toughness of the hardmetal inserts. The inserts must have the ability to resist micro-cracking and this is related to fracture toughness.

Hack and Peters (1985) report that, although abrasive wear can be dominant during rock drilling, another important contribution to the wear arises from the high energy impact needed for the fracturing of the rock. The following diagram is a schematic of the type of insert that was used in the testing performed by Hack and Peters (1985).

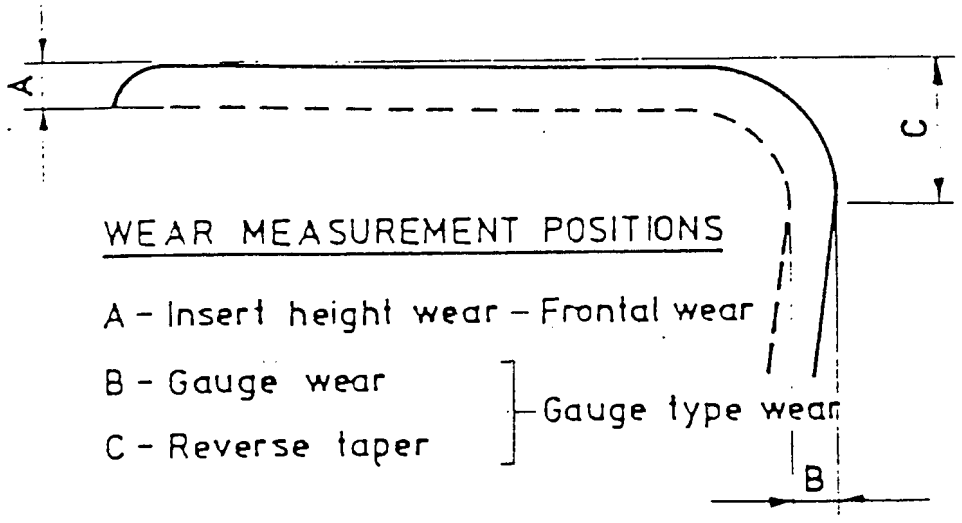

Figure 2. Cross-section of chisel-shaped cutting insert (after Hack and Peters 1985)

In fig. 2. the upper gauge portion of the insert suffered material loss by sliding abrasion (from rotation) and impact fatigue spalling (from percussion).

Hardness was not a fundamental parameter controlling wear resistance in the rotary-percussive testing of the above report. The main cause of wear is said to be impact spalling. This impact spalling occurs by initiation and propagation of localised micro-cracks under the action of an impact stress. Joining up of the micro-crack systems leads to the removal of a small particle of hardmetal (Hack and Peters [1985]).

According to Montgomery (1968) and (1969), the resistance to wear **at a particular** hardness level increased with increased mean-free path of the binder phase. Since surface impact spalling is a fracture process, low cobalt grades may be expected to wear fast due to impact spalling. Low cobalt grades have a lower fracture toughness and this would encourage impact spalling. Larsen-Basse (1973) reports that when drilling hard rocks frontal wear by impact and impact fatigue can dominate. He believes wear resistance is not a simple function of hardness, cobalt

content and mean-free path alone but that the type of rock drilled is also of importance.

According to Larsen-Basse (1973) the transition between damage due to larger spalls and smaller ones occurs at around 12% cobalt for fine grained WC-cermet (1-2μm) and around 8% cobalt for a WC grain size of (2-4μm). The size of the spalls was evaluated qualitatively by visual inspection. This transition occurs at a hardness of 1440-1450Hv and a mean-free path of 0.35 to 0.4 μm. Larsen-Basse (1973) concludes that this indicates the mean-free path is an important parameter. McLaren and Lambert (1981) state that binder mean-free path is related to the plane strain bulk fracture toughness of the hardmetal and that thicker layers of binder can blunt advancing cracks better due to lower internal stresses. Hack and Peters (1985) conclude that wear by impact microspalling will increase with decreasing bulk fracture toughness but that in rock drilling, abrasive wear processes can be dominant.

It appears from the above paragraphs that mean-free path and/or fracture toughness are important for spalling resistance. A marked change in flake size at a certain mean-free path and hardness is also reported. These findings are similar to some of the results of the repetitive impact testing that will be presented later i.e. influence of mean-free path and the distinct change from large spalling to smaller spalls. Repetitive impact testing therefore appears to predict to some extent, when microspalling will occur. It has, however, been noted by Larsen-Basse (1973) and Hack and Peters (1985) that abrasive wear processes can have a dominant influence on the total wear occurring during rock drilling. Repetitive impact testing can thus not be used in isolation to predict wear occurring during percussive rock drilling.

Impact Testing

Brittle materials are used for many machining applications including rock cutting, metal cutting, dies and forming tools. Unfortunately brittle materials are susceptible to edge flaking which can become a major life limiting factor for these tools. A compromise has to be found for the shape of the cutting edge. To have an efficient cutting surface a sharp edge is necessary while for tool longevity this edge needs to be blunt (N.J. Mc Cormick, [1992]). Hard cutting materials need to have a good resistance to edge flaking so that a sharp edge can be maintained; therefore a knowledge of their edge toughness is essential.

Edge Flaking

Damage occurring to an edge by point loading is dependent on the magnitude of the load and the distance from the edge that the loading is applied.

McCormick and Almond (1990) state that the geometry of a flake was found to be material independent while the load required to produce the flake had a strong material dependency.

McCormick and Almond (1990) chose a model developed by Jeffrey (1920) to describe the position of crack initiation for an edge indentation system. They analysed the stress field set up by the finite contact zone between a loaded indenter and the indented surface in an attempt to understand and explain the features of edge flaking. The stress analysis that was used was of an semi-infinite, internally pressurised cylinder close to the surface of a semi-infinite solid.

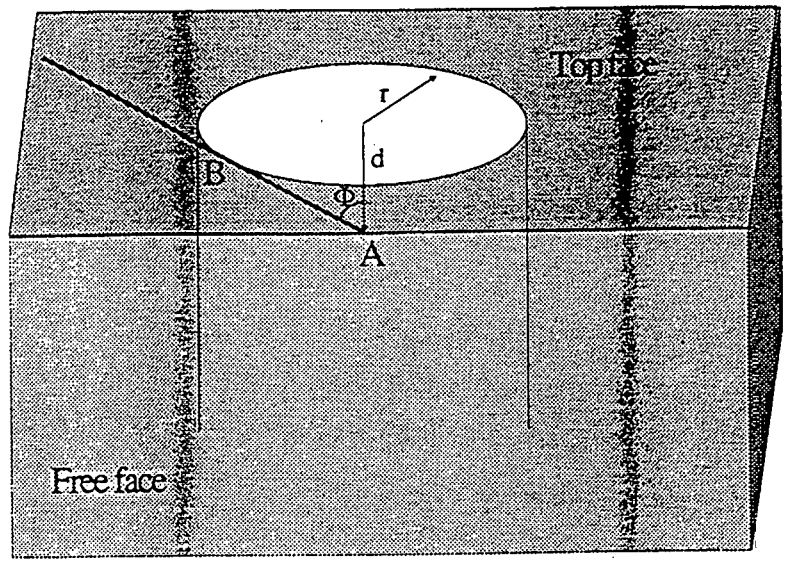

Figure 3. Maximum hoop stress at position B (after McCormick and Almond 1990)

McCormick and Almond (1990) summarise the stress analysis as follows:

Displacement of edge at position A

$$U=[Pd(v^2-v-2)r^2]/[E(d^2-r^2)] \quad (1)$$

Maximum stress on edge of hole, position B

$$\sigma_B=P.[(d^2+r^2)]/[(d^2-r^2)] \quad (2)$$

Maximum stress on edge of specimen at A

$$\sigma_A=4Pr^2/(d^2-r^2) \quad (3)$$

Using a geometrical construction the position of maximum stress can be found. The maximum stress occurs on the boundary of the cylinder, at position B, where the tangent to the indentation passes through the symmetrical point at position A. It can be seen from the comparison of equations (2) and (3) that the maximum stress occurs at position B as illustrated in fig. 3. only if the distance from the edge was greater than $\sqrt{3}.r$ i.e. if equation (2) has a greater value than equation (3). When this condition is not met the crack will start perpendicular to the free surface of the specimen and travel inwards towards the centre of the

contact zone. This condition ($d>\sqrt{3}.r$) may not be met for soft materials where the indentation contact area is large.

This condition ($d>\sqrt{3}.r$) was met for the repetitive impact testing of the WC-cermets and the glass although a groove was introduced to lower the energy needed to cause a flake to be formed (this is illustrated in fig. 14. under "Experimental Procedure").

McCormick and Almond (1990) showed further that the ratios of maximum width of flake to depth of flake and also maximum width of flake to thickness of the flake are independent of the material indented. According to them this implies that for elastically isotropic materials the flake geometry is due to the stress field produced by the indenter.

McCormick (1992) states in a more recent paper that the dimension ratio of the flakes produced from many different materials with widely different toughness were very similar.

McCormick and Almond (1990) report that flakes formed at rectangular edges follow a law of constant geometry. This conclusion was drawn after they had indented rectangular blocks under increasing loads at different distances from the edge. They observed that the size of flakes formed in a tungsten carbide-cobalt tool material decreased with a decrease in distance from the edge and the width to height and thickness-to-height and ratios of the flakes were approximately constant.

Dynamic loading does appear to be markedly different to static loading in at least one particular aspect. As is reported later, in the thesis, the dynamic loading testing carried out by the author shows a strong material dependency for the size of the flake while according to McCormick and Almond (1990) with

flakes formed due to static indentation the size of the flake depends only on the distances of the loading point from the edge and is relatively independent of the material. Results of the testing carried out by McCormick and Almond (1990) are illustrated in the following figure. They show a straight line relationship between depth of the flake and distance from the edge that the indent occurred, for a variety of materials.

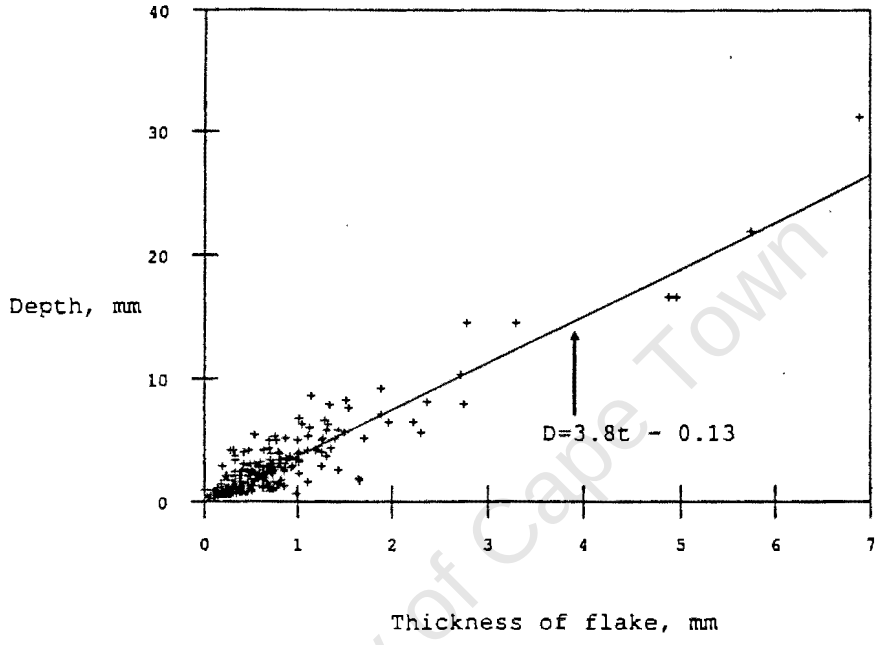

Figure 4. The depth versus the thickness or distance from the edge of a flake for a variety of materials (after McCormick and Almond 1990)

Cotterell, Kamminga and Dickson (1985) stated that unless the direction of the flaking force is appropriate the crack forming a flake hinges outward immediately towards the surface of the core (block from which the flake is removed) or plunges inwards towards the centre of the core. The direction of the force required to keep the crack parallel to the surface of the core varies with the growth of the crack. The stiffness of the partially formed flake dictates that the line of force will be close to the angle required to cause the crack to propagate parallel to the surface of the core. When the crack hinges towards the free surface the negative bending moment caused by the direct component of the force increases which in turn causes the crack tip stress intensity to

become positive causing the crack to deflect back towards a parallel path. According to them crack intraflection into the body of the core has a similar correcting mechanism resulting in undulations on the fracture surface. Fig. 5. below illustrates these undulations as well as the bulb of force or percussion.

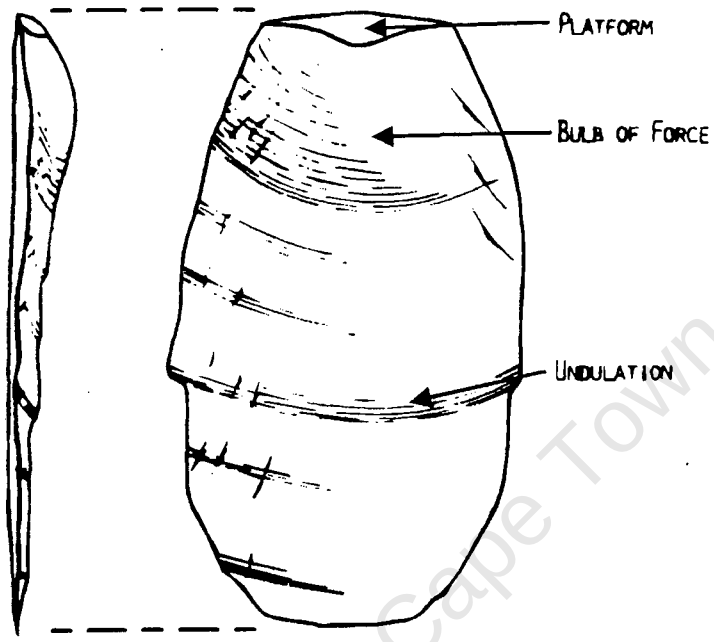

Figure 5. An edge flake (after Cotterell et al 1985)

According to Thouless, Evans, Ashby and Hutchinson (1987) three types of stress intensities can occur at a crack tip as illustrated in the following figure.

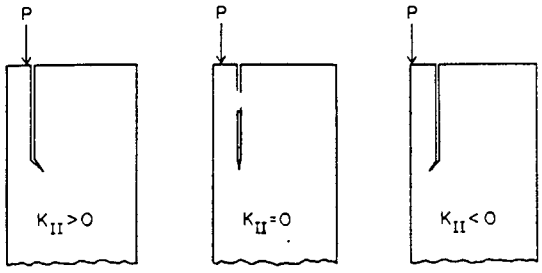

Figure 6. The effect of K11 on crack path (after Thouless et al 1987)

In theory a positive stress intensity causes the crack to travel into the impacted block while a negative stress intensity causes it to travel out of the block. Erdogan and Sih (1963) report that, in brittle solids, a planar crack only continues to advance in its own plane when the crack tip is subject to pure mode I.

In practice, however, according to Thouless et al (1987) friction Q at the contact point of the force P, as illustrated in the figure below, causes the force system to change. This frictional force Q develops as the specimen attempts to rotate in response to the imposed moment M. The imposed moment M is set up due to the tendency for the flake to buckle.

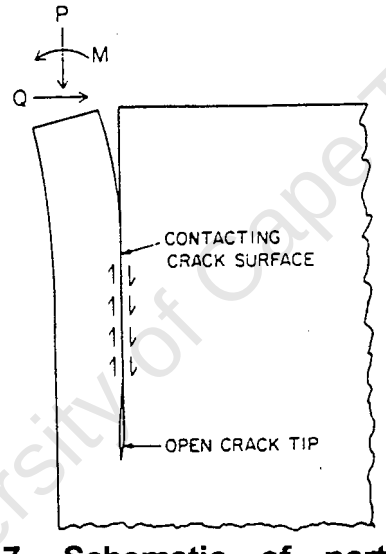

Figure 7. Schematic of partial crack surface contact (after Thouless et al 1987)

This frictional force Q inhibits the full transmission of the imposed stress intensity to the crack tip, causing the crack plane to become closer to the surface. Edge spalling is therefore attributed by them to the onset of elastic buckling for the reason that buckling induces a negative crack tip stress intensity, which in turn causes the crack plane to be deflected to the surface. It must be noted that the model proposed by Thouless et al is for loading on the

top surface of a flake. This is a slightly different situation to when the flake is formed by a sharp indenter.

Edge Toughness

McCormick and Almond (1990) deal with the question of edge toughness and put forward the formula: L=Md where L = critical load for edge flaking

M = a material constant

d = distance from the edge

They state that when an indenter was loaded at a given distance from the edge of a block there was a critical load at which failure occurred. It is further explained that the fracture load was approximately proportional to the distance of the indenter from the edge. This constant of proportionality can therefore be related to the material. M is the ratio of the flaking load to the distance of the indenter from the edge and is a measure of the edge toughness of a specific material. Materials with a different value of M are illustrated in the following figure.

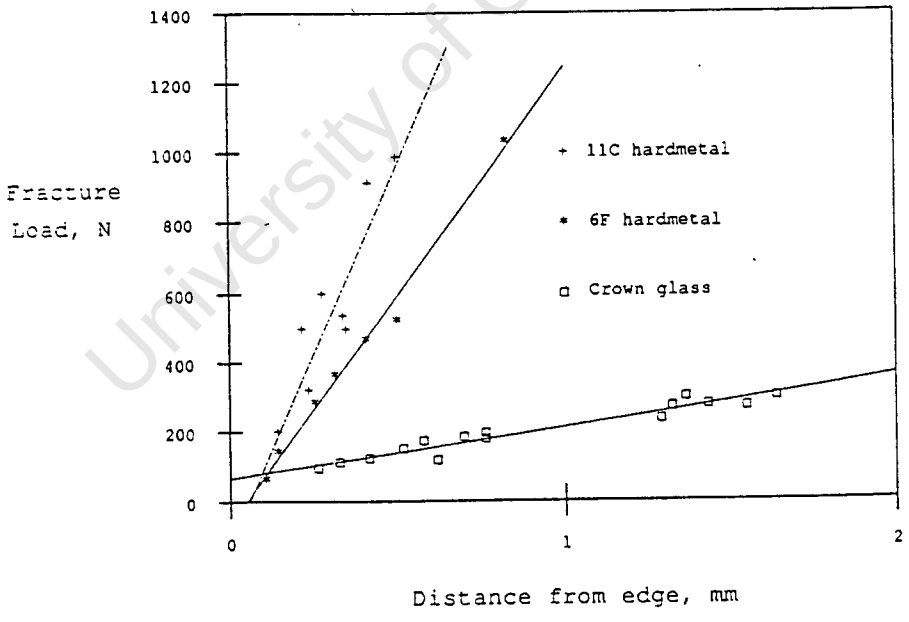

Figure 8. The load to produce a flake versus load application distance from edge of specimen (after McCormick and Almond 1990)

McCormick (1992) reports in a further paper that within experimental error there is a clear monotonic relationship between edge toughness M and G_{1c}, and thus K_{1c}. G_{1c} is the critical strain energy release rate and is related to fracture toughness K_{1c} and Young's modulus E, by the formula $G_{1c}= K_{1c}^2/E$. Fracture toughness can therefore be calculated from the edge toughness of the material.

Hertzian Fracture

Ogilvy, Perrott and Suiter (1977) state that the most common form of indentation fracture in a brittle solid is the Hertzian cone crack. This fracture mode occurs on contact between two curved bodies or when a rigid sphere is loaded against a flat slab of brittle material. Auerbach's law states that when a hard spherical indenter is pressed with an increasing normal force P on to the flat face of a brittle solid, a cone crack develops after P reaches a critical value P_C. P_C is found to be proportional to R i.e. as R increases so P_C increases.

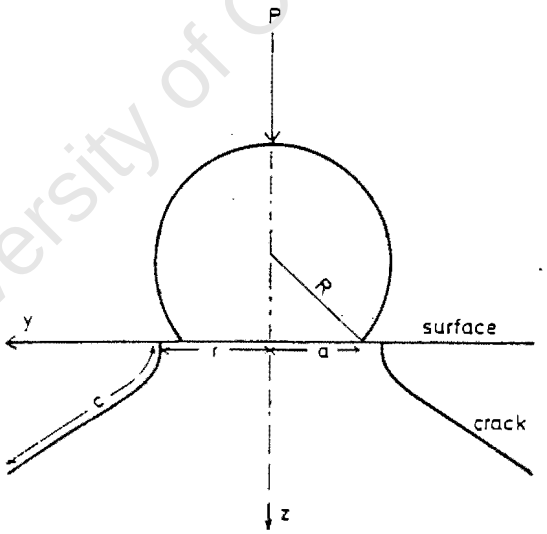

Figure 9. Vertical centre section showing Hertzian indentation geometry

Roesler (1956) demonstrated the equivalence of the empirical relationships between slowly applied and impact loaded Hertzian cone cracking. These two conditions can be considered to be the same as what occurs just before

fracture, where the elastically stored energy is proportional to the area of the circle of contact.

The formulas describing this Hertzian stress system where first developed by Hertz in 1881 and have been quoted, not only by Frank and Lawn (1967), Wilshaw (1971), Warren (1978) and Fischer-Cripps and Collins (1994) but by many others, in the following forms:

$$a^3 = 4kPR/3E$$

where P = indentation load

a = radius of the circle of contact

E = Young's modulus of the sample

R = indenter radius

The constant $k = 9/16[(1-\nu^2)+(1-\nu'^2)E/E']$

where ν = Poisson's ratio of the sample

ν' = Poisson's ratio of the indenter

E = Young's modulus of the sample

E' = Young's modulus of the indenter

The tensile stresses in the sample are proportional to the average contact pressure $P/\pi a^2$. In the region below the indenter the stresses are compressive while outside the contact circle a radially directed tensile stress is created at the sample surface (z=0) such that:

$$\sigma(y,z=0) = [(1-2\nu)P/2\pi a^2](a/y)^2$$

Thus the formula predicts the tensile stress is a maximum at the circle of contact. The Hertzian cone crack, however, does not start at this circle of contact (radius a) but at a circle of radius r as illustrated in the above figure.

The repetitive impact testing reported on in this thesis gave rise to, amongst other crack types, Hertzian cone cracking in the glass and the WC-cermet test blocks.

Impact of Glass

Glass is a brittle material (fracture toughness of 0.8MPa$\sqrt{m}$) and was considered to be a good material to model the cracking that was observed to occur in the WC-cermet test blocks. Ball and Mc Kenzie (1993) reported observing Hertzian cone cracks, median, radial and lateral cracking on the contact surface of edge clamped glass plates subjected to low velocity impact. These crack types where also observed by Swain and Hagan (1976) while using a universal testing machine which gives a quasi-static type of loading.

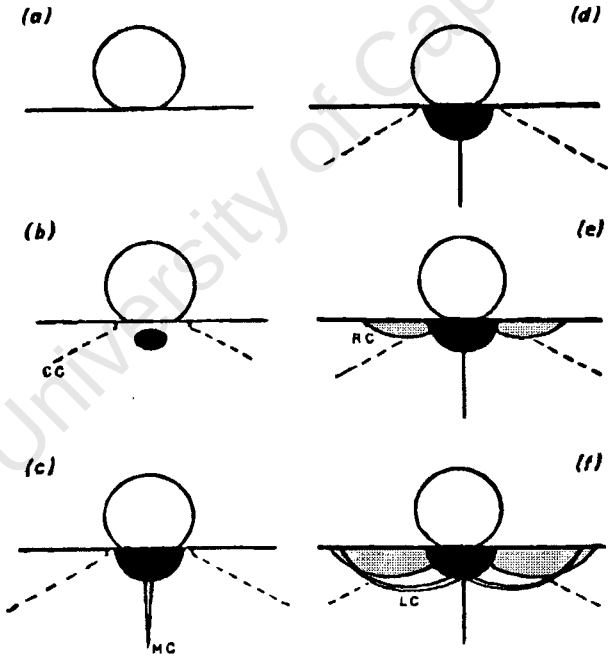

Figure 10.: Schematic diagram of the cracking occurring during a loading-unloading cycle with a small spherical indenter (after Swain and Hagan).

Fig. 10. is an illustration of the cracking observed by Swain and Hagan during indentation of glass. The glass is being progressively loaded from diagram (a)

to (c) and unloaded from diagram (d) to (f). Median cracks (MC) as well as plastic deformation (dark zone) and occasionally Hertzian cone cracks (CC) form during the loading cycle. Radial cracks (RC) and lateral cracks (LC) occur on the unloading cycle.

Tsai and Kolsky (1967) reported a similar phenomena when impacting glass plates with a steel ball. They stated that the Hertzian cone fracture grew and penetrated further into the glass plates as the impact velocity increased. At higher velocities two or more Hertzian cone cracks were formed and radial fractures also appeared; these eventually fractured the whole specimen. Also at the highest velocities they observed a powdering of the glass surface immediately under the centre of the impact. They assumed that the crushing was due to a multitude of tiny cracks which were caused by the presence of a large compressive stress.

The shape of the indentation head does appear to have an influence on the type of cracking that will occur. "Blunt" indenters can cause different cracking to "sharp" indenters.

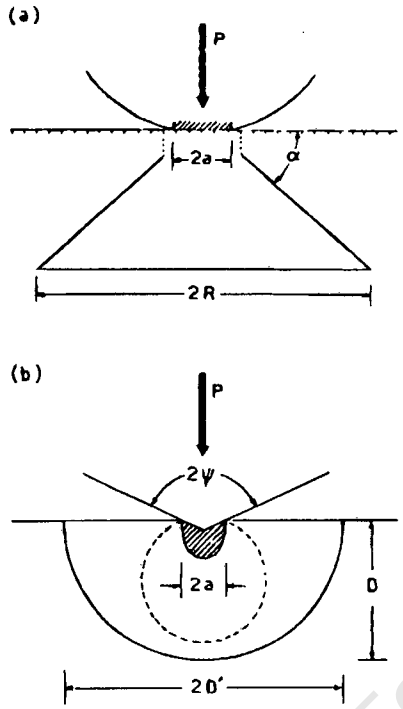

Figure 11. Basic indentation fracture systems (after Lawn and Fuller, 1975)

Diagram (a) in fig. 11. is a cone crack system, associated with a "blunt" indenter and (b) is a median crack system, associated with a "sharp" indenter. According to the above diagram the cone crack in (a) nucleates from a pre-existing surface flaw (small dashes) outside the contact area and forms into a surface ring (broken line), and finally becomes critical and propagates into a fully developed cone. The median crack in (b) nucleates from the plastic contact zone (shaded) and forms into a contained penny (broken circle) and ultimately develops into a full half penny.

Experimental Procedure

A common method to measure the edge toughness of a cutting material is to subject it to a load on an edge that causes a flake to break off. In these tests a block shaped specimen is clamped on a stage (fig. 12.) and an indenter (e.g. Rockwell) is pressed into the block at one of the edges until a flake is formed.

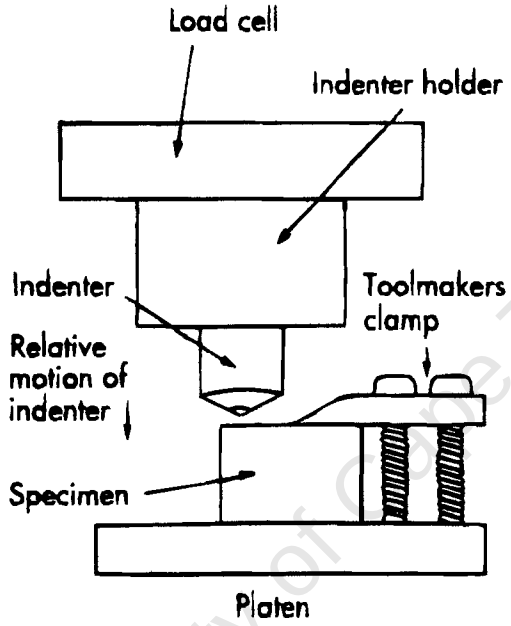

Figure 12. Quasi static loading (after N.J. Mc Cormick, 1992)

The load at which the flake is formed is then recorded. To give a measure of the edge toughness of the material, the load and the flake size are used in an empirical relationship.

In an attempt to obtain a situation closer to practice and to study the crack growth mechanisms involved during edge flaking it was decided not to use the above method to edge flake the material. Dynamically loading the specimen gives rise to crack growth regimes that are more representative of what occurs during fracture of metal machining or rock cutting tools.

A repetitive impact method was chosen. The testing involved repeatedly striking a test block at a single position close to one edge. The impact energy, for each blow, remained constant during a test but was varied for separate tests.

Test Equipment

The rig consists of a rocker arm raised against the resistance of a spring by a rotating cam (fig. 13.).

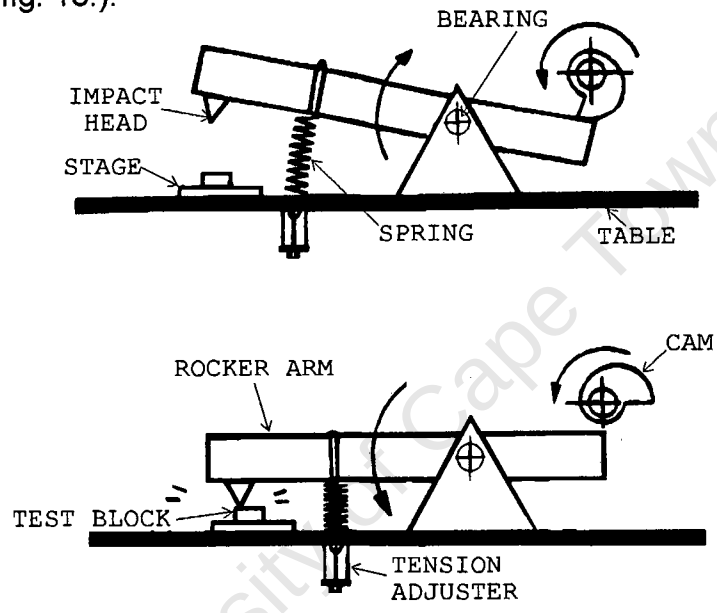

Figure 13. Diagram of impact rig

A motor is mounted on a steel table and by means of a belt, drives a camshaft. The cam accentuates a rocker arm that is pivoted on two bearings. As the rocker moves up and down an impact head strikes the test block that is fixed in position on a stage. The energy with which this head strikes the test block can be set by adjusting the pretension of a spring attached to the rocker arm. The energy range of the impacting is 0 to 10 Joules. The amount of impacts is recorded by a sensor that counts the number of revolutions of the camshaft. The impact frequency can also be set from 1-15Hz by adjusting the speed of rotation of the motor.

Modifications were made to components of the rig to cope with both the testing of the extremely hard and tough WC-cermet and fragile glass test blocks. A stage was designed to hold the test blocks in place and allow the impact head to strike at any fixed distance from the front edge of the test block.

An optical fibre cable had to be incorporated into the stage before impact testing could commence. This was done for two reasons. Firstly to prevent further damage to the impact site after a flake had formed and secondly to prevent excessive damage to the impact head. If the impacting was not stopped immediately after the flake had formed the head would come down on a sharp edge of the test block and damage would occur to both itself and the impact site.

The optical fibre cable reflects a beam along the front face of the test block and this beam is received by another optical fibre cable which is attached to a sensing unit. When a flake forms and is removed from the front face of the test block the beam is broken and the impacting is stopped.

The selection of the optimum material for the impact head proved the greatest problem. The high hardness and toughness of WC hardmetals makes it necessary to induce a very high stress level in the surface of the test block in order to initiate a crack. Thus the area of the impact head that comes into contact with the test block must be small and the force of impact must be high. It was decided that the heads must have a conical shape with a radius of 1mm at the tip of the cone. This shape is a compromise between wear of the impact head and the above requirement.

Numerous steels where tested for the manufacture of the impact heads. These included various tool steels i.e. En 24 and En 30B. These steels were quench hardened to 450Hv however they would deform badly at any impact energy above 3J. Some high carbon steels with carbon levels of 1 weight percent and

above were tried. Although these steels can be hardened they are too brittle and the heads crack during impacting.

A tungsten carbide impact head was obtained from Boart Research Centre and used for impact but it suffered severe damage due to cracking. The head was made of a 15% cobalt binder grade which is more resistant to brittle fracture than the lower cobalt grades.

Eventually a cold work isomatrix powder metallurgical steel was decided upon. The composition of this steel is 2.3%C, 12.5%Cr, 1.1%Mo, 4%V, 0.4%Mn, 0.4%Si. It is produced by sintering and it can be hardened to 950Hv. When tempered back to 800Hv it gives excellent toughness. Although this steel still suffers some damage during impacting it is the best material used to date.

Materials Tested

Eight industrial grades of this cermet were supplied by Boart Longyear Research Centre (BLRC); Krugersdorp. The material to be tested was supplied in various binder percentages, binder types, and grain size. For the cobalt binder grades, the grades designated "S" have a finer grain size than those designated "G". Except for grade V7 the number in the grade designation refers to the percentage, by weight, of binder. These properties have been measured by BLRC. The table below details some of these properties:

Grade	Binder wt %	Binder Type	Frac. Tough. MPa√m	Hardness Hv_{30}	Grain Size µm
S6	6	Co	10.4	1550	1.3
G6	6	Co	13.7	1350	2.3
S10	10	Co	12.6	1350	1.2
G10	10	Co	15.3	1230	2.0
S15	15	Co		1180	1.6*
G15	15	Co	16.2	1070	2.4
V7	6	Ni-Cr	9.8	1600	2.0
P15	15	Ni-Cr-Co	17.0	1050	2.3

Table 1: Grades supplied for testing

The sintered test blocks were ground to a size of 10mm×10mm×20mm (fig. 14.). A 0.1mm deep groove was machined parallel to a long face of the test block at a distance of 0.7mm in from this edge. The groove was 0.5mm wide. The impact occurred directly above and in the centre of the groove.

* Obtained from coercivity measurement

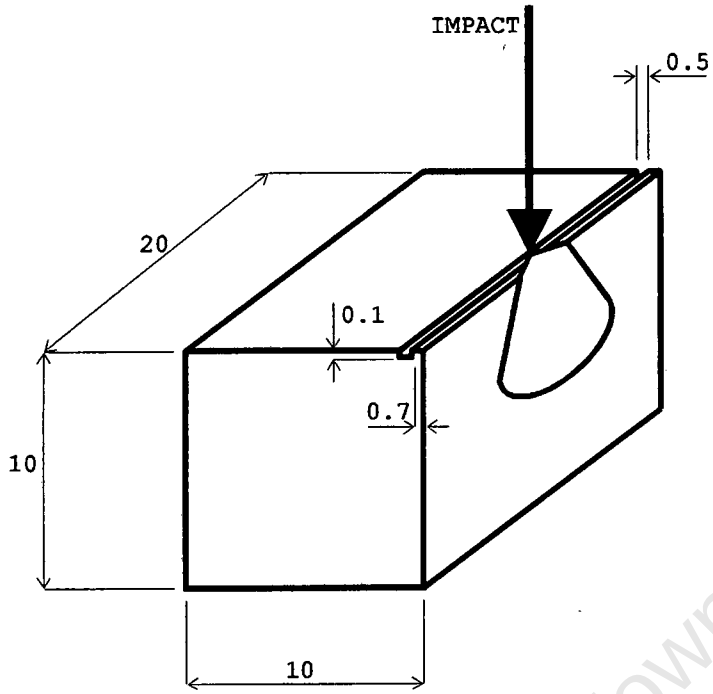

Figure 14.: Test block with impact site 0.7mm from front face

This groove facilitated the initiation of the flake formation at a lower impact energy. The machining of the groove causes small flaws to be left behind which act as crack initiation points. The radius of the groove has a stress raising effect which also facilitates cracking.

It was necessary to lower the impact energies, by introducing the groove, to prevent premature failure of the impact head. The introduction of the groove had no influence on the geometrical shape of the flake. It is thus not considered to adversely influence the results of this testing.

Test schedule

After the initial testing it was discovered that grades with different binder contents had different threshold impact energies for fracture. By threshold impact energy it is meant the minimum energy for flake formation within 500 impacts. Each grade was impacted between 0.25J below and 0.5J above this threshold at energy increments of approximately 0.1J

This sequence of testing was performed three times for each grade using a new head each time to minimise the influence of head damage on the testing.

The individual impact tests carried out at each energy level continued until a maximum of 500 impacts or the until flake was fractured off the test block. The frequency of these impacts was set at 2Hz.

Evaluation of the flakes

Each test block that was impacted was weighed before and after impacting. The mass of a flake that formed during impacting could thus be determined. Every test block was photographed from the top (impact site) and from the side (face where flake was removed) in order to record of the shape of the flake before any sectioning for microscopic investigation was undertaken.

Optical and scanning electron microscopy

The crack growth paths and the fracture surfaces of the flakes and their parent test blocks were studied using a various microscopy techniques.

Optical microscopy

The macroscopic crack growth paths that occur just before failure (removal of the flake) were studied by cutting cross-sections through the impact site of the test block from each grade. These test blocks had been impacted to a point where the flake was on the brink of removal.

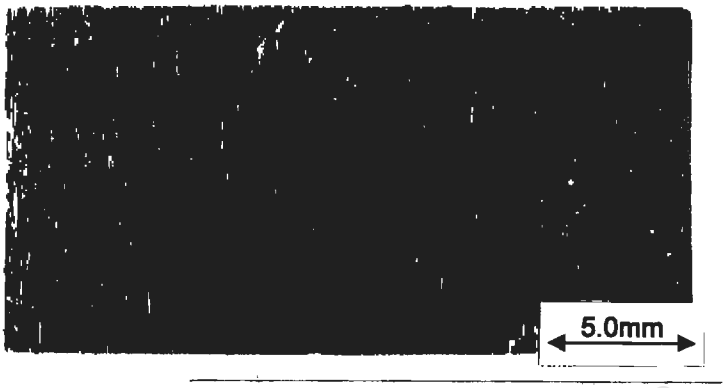

Figure 15. Front face of a WC- cermet test block showing a flake on the point of removal

The test block was mounted in resin to hold the flake in place. After mounting the test block was then sectioned using a diamond cutting wheel with the cut passing through the centre of the flake. The cross-section surface was then polished to a finish of 1μm using diamond paste. The polished surface was not etched thus avoiding removal of binder from the vicinity of the crack.

This polished surface was then photographed though an optical microscope in order to record the length and shape of the cracks.

Scanning electron microscopy

Back scattered electron microscopy (BSE):

These cross-sections, discussed above, were then studied under high magnification using the BSE technique.

Impingement of the electron beam on the target causes most of the electrons expend all their energy in the interaction volume. They are

absorbed by the target [Goldstien, Newbury, Echlin, Joy, Fiori and Lifshin (1981)]. A small percentage of these electrons are scattered out of the specimen and these are collectively known as back scattered electrons.

This technique is useful when studying WC-cermets since the number of electrons that are back scattered increases with an increase in atomic number of the target. The high atomic mass of tungsten in the tungsten carbide particles causes the scattering of significantly more electrons than the metallic binder phase. There is thus a very clear distinction between the tungsten carbide particles and the binder phase. The crack growth path can therefore be clearly seen.

The WC-cermet grades were studied using this BSE technique in order to determine to what extent the crack growth paths were intergranular or transgranular.

Secondary electron microscopy:

The fracture surfaces of the flakes and the test blocks were studied using the secondary electron technique.

The secondary electron coefficient is relatively insensitive to composition and fails to show a significant trend with change in atomic number [Goldstien et al (1981)]. The secondary electrons, however, give a better image of local topography of the fracture surface being viewed.

Therefore in an attempt to understand the crack growth paths in the various grades the secondary electron technique was used to study the topograghy of the fracture surfaces.

Modelling of macroscopic crack shapes using glass

In order to understand the crack shapes that were evident in the WC-cermet test blocks it was decided to impact glass. Glass is a well researched material and much is understood about the types of cracking that occur in it. It also has the added advantage of being transparent, making the internal cracking easy to study.

Glass test blocks were prepared by cutting them with a diamond saw to the same size as the WC-cermet test blocks. The adjustable stage was used to move the point of impact on the glass blocks in increments of 1mm, for each successive test, until the impact was made in the centre of the test block. The test blocks were impacted at various energies at each of these points.

Each impact test was carried out at different a energy and distance from the edge. The impacting always occurred on the float or air surface of the glass where surface finish is good and the number of flaws to initiate cracking is uniform.

These tests were carried out to determine how the cracking in the centre of the test block altered as the impact site approached the same position at which the WC-cermet test blocks were impacted i.e. 0.7mm from the edge.

Furthermore, a groove was scratched, using a diamond pencil, along the edge of the glass block in a similar place as the slot in the WC-cermet test block to observe how this would influence the crack shape.

Results

Impact of Glass

The following results are obtained by impacting at different energies and distances from the edge of the test block. The number of impacts, before failure, is recorded in table 2. Impacting was only carried out to a maximum of 1000 impacts. In the event that no failure occurs, before the maximum number of impacts is reached, a figure of 1000 is recorded.

Distance from front face (mm)	Impact Energy (J)										
	0.15	0.30	0.45	0.59	0.74	0.89	1.04	1.19	1.34	1.48	1.63
5.3								1000	1000	567	16
4.7								1000	1000	1000	22
3.7							1000	1000	39	14	2
2.7						1000	1000	1000	70	63	4
1.7				1000	1000	23	31	1	2	2	1
0.7	53	38	16	7	6	1	1	1	2	1	1

Table 2: Glass impact results

The following map of the crack types that occur in the glass test blocks has been obtained from the data of the preceding table.

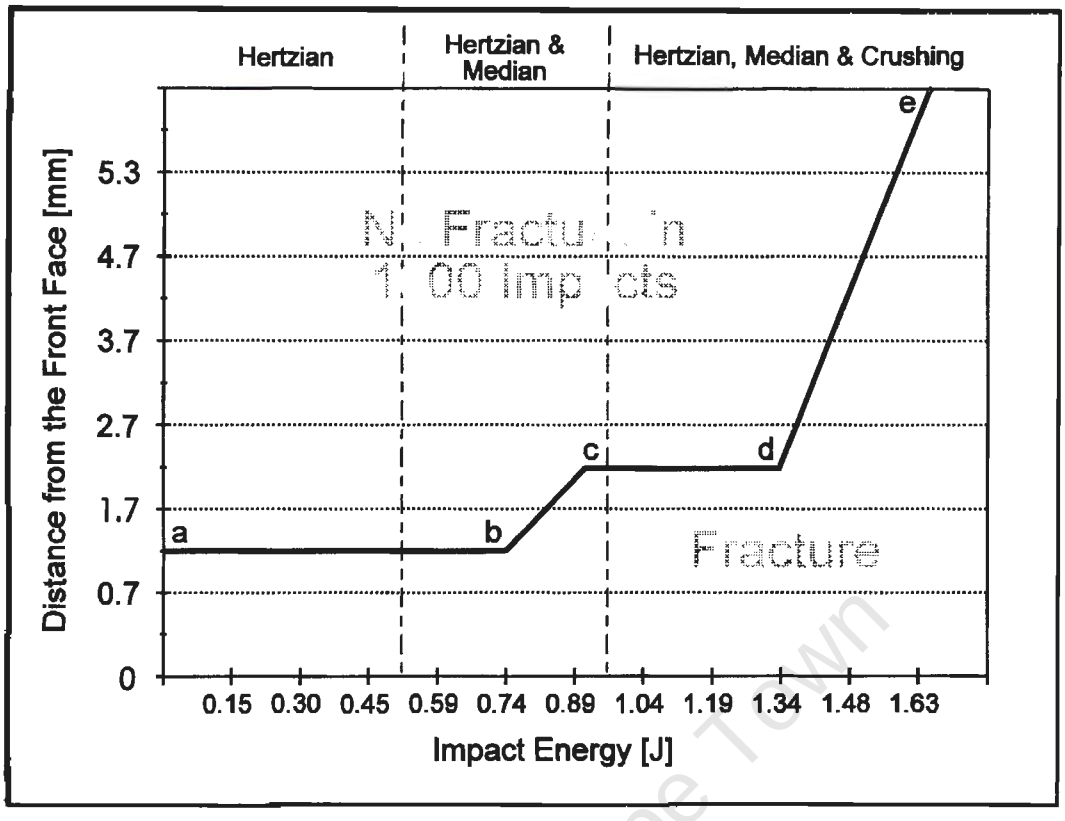

Figure 16.: Map of crack types formed during impact of glass

The above figure graphs the impact energy versus the distance from the front face into the test block at which the impacting occurred. The impact energy is recorded on the x-axis of the graph above. The distance that the impacting occurred from the front face is recorded on the y-axis. Above the line abcde no failure occurs in 1000 impacts while below the line failure does occur after less than 1000 impacts. The test block is considered to have failed when it splits into two or more pieces. When a flake does form it will occur in substantially less than 1000 impacts; usually in the range of 1 to 100 impacts. Below the line, for each distance into the test block, the number of impacts to failure decreases as the impact energy increases but this has been omitted to simplify the diagram. From an impact energy of 0.15J to 0.45J the failure or cracking that occurs at all distances or impact positions into the test block is purely Hertzian. From 0.59J to 0.89J the failure or cracking seen is both Hertzian and median while from 1.04J to 1.63J Hertzian, median and crushing are evident. For all the glass impact tests an increase in energy changes the crack type from

Hertzian into Hertzian and median cracking. Although lateral cracking occurs at and above 0.74J it has also been omitted to simplify the diagram.

Impact in the centre of the test blocks

At high energies there is a high degree of crushing at the impact site. The crushing can be seen as an opaque white area and this white colour is a result of the formation of many inter-linked cracks. The crushing region persists down to an energy of 1J. This opaque crushed area can be seen in fig. 17.

Figure 17. Top view of a test block impacted in the centre at an energy of 1J

Median cracking is also evident and persists down to a lower energy than the crushing. The median crack type is found down to as low as 0.6J. At 0.6J the size of the median crack (A) is the smallest observed and this is illustrated in fig. 19.

At energies from 0.45J to 0.15J only Hertzian failure is evident. The size of the Hertzian cone decreases with a decrease in impact energy. This Hertzian cone is illustrated in fig. 18. and the cone is at its smallest observed since the impact has been done at the lowest energy of 0.15J.

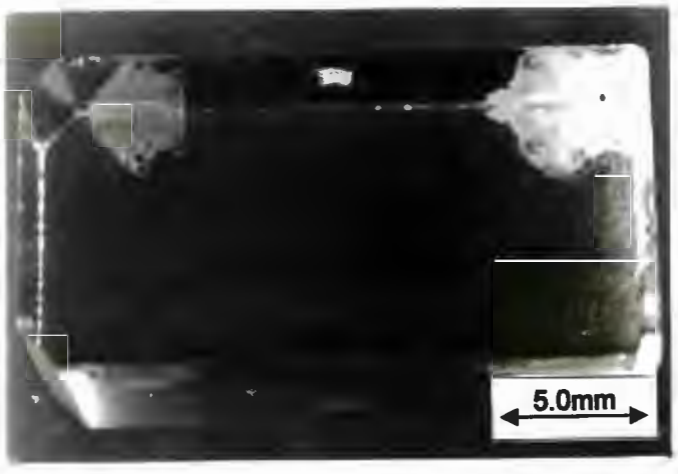

Figure 18. Side angled view of a glass test block impacted in the centre at an energy of 0.15J

At impact energies from 0.45J to 1J a Hertzian cone is evident but it occurs in combination with a median crack. This is illustrated by fig. 19. and fig. 20. where the Hertzian cone is designated by the letter B and the median crack by the letter A. In fig. 20. the impacting has occurred at an energy of 1J while in fig. 19. the impacting occurred at an energy of 0.6J.

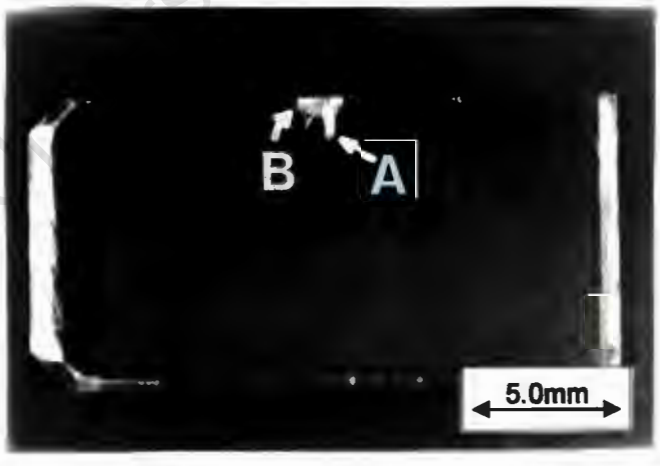

Figure 19. Side view of a glass test block impacted in the centre at an energy of 0.6J

The median crack (A) can be seen to intrude deeper into the test block than the Hertzian cone (B). Impact at a higher energy causes the median crack to increase in size as shown in fig. 20.

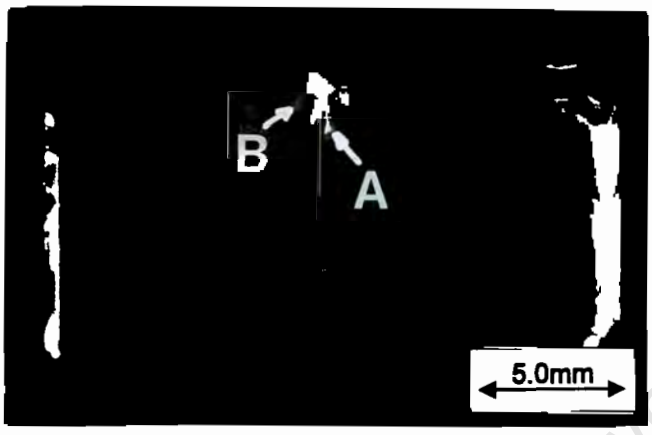

Figure 20.: Side view of a glass test block impacted in the centre at an energy of 1J

The Hertzian cone (B) is also larger in fig. 20. than in fig. 19. With an increase in energy the median crack becomes more dominant and it eventually causes the failure of the block when the impact is confined to the centre of the test block. The median crack propagates through the test block causing it to fracture.

Hertzian cone cracking appears to occur at all the impact energies but at energies from 1J and above it is obscured by the crushing surrounding the impact site. Fig. 21. illustrates the remnants of a Hertzian cone (B) after the impact had split the test block in two.

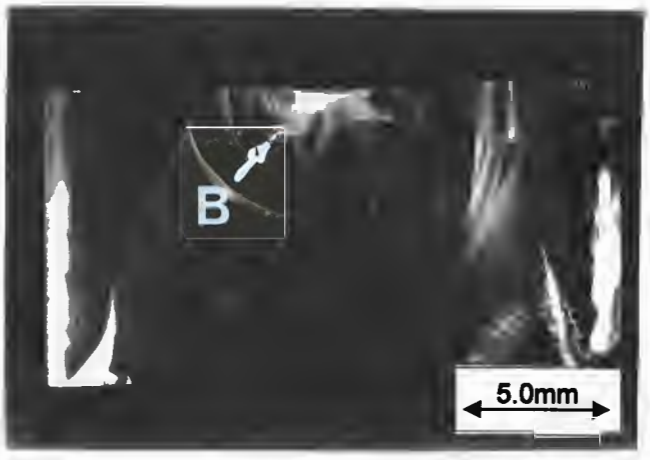

Figure 21.: Side view of a glass test block impacted in the centre at an energy of 1.5J

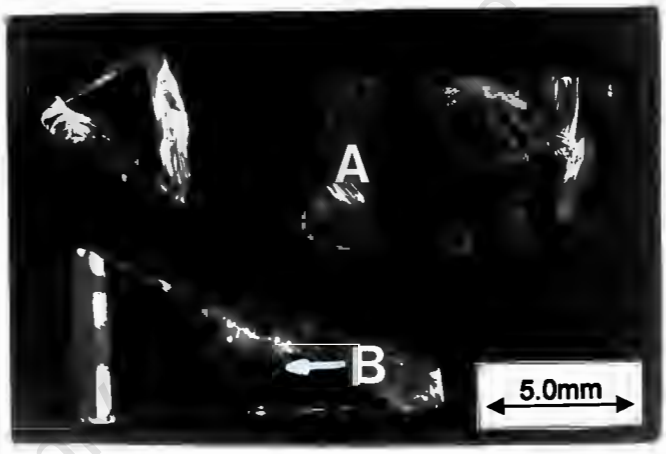

Figure 22. Glass test block impacted in the centre at an energy of 1.6J

A test block that has been split into three pieces, by impact in its centre, can be seen in fig. 22. The semi-circular lines (A) are left behind by the median crack on the fracture surface. A high degree of crushing can be seen at the impact site and this may have obscured the presence of a Hertzian cone crack. Some lateral cracking (B) can be seen around the impact site. Lateral cracking is always evident above an impact energy of 0.74J.

Impact 0.7mm from the front face of the test block

Impact at this position shows the same crack types, in the same energy ranges, as impact in the centre. At this position there is fracture at all the impact energies while impacting glass. This impact position is the same position that was used for the impacting of the WC-cermet test blocks.

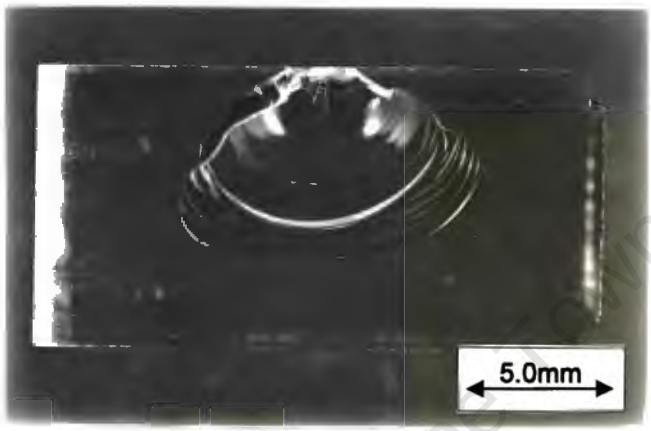

Figure 23. Side view of a glass test block impacted 0.7mm from the front face at an energy of 0.15J

The flakes that form here have a truncated conical shape, due to the ring crack intersecting the front face, and are symmetrical about the test block centre axis. An illustration of the impact site and the truncated cone, that is formed in both glass and WC-cermets (see later), is shown in fig. 14 (see Materials Tested section). By referring to the map of crack types, in fig. 16, one can see that pure Hertzian cracking is only responsible for the cracking below 0.6 J. One therefore does not see flaking where the ring crack is fully contained within the test block (during impact at distances of 1.7mm or higher) because the fracture is dominated by median cracking. Unlike the cracks in the centre of the test block the flake that forms on the edge of the glass test block does not show a large difference in size at different energies when the fracture occurs in the pure Hertzian range i.e. at energies below 0.6J. The mass (size) of the flake is

not dependent on the energy of impact in the Hertzian range. It will be shown later that the mass (size) of this flake is dependent on the material being impacted.

At energies from 0.6J to 0.9J the edge flake fracture is caused by both Hertzian (B) and median cracking (A). In fig. 24. the median crack (A) is obscured by a conical shaped Hertzian fracture (B).

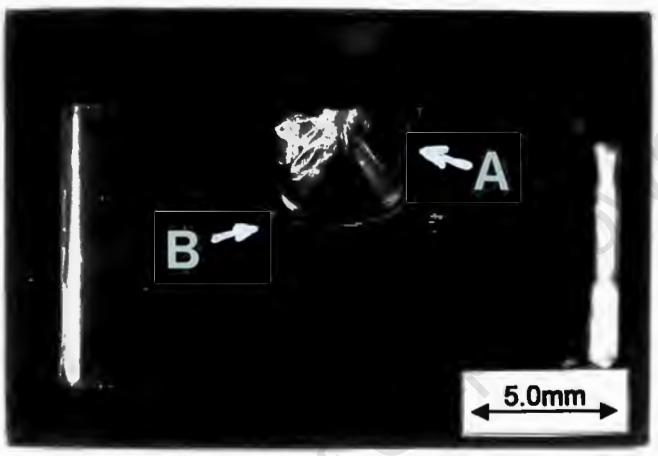

Figure 24. Side view of a glass test block impacted 0.7mm from the front face at an energy of 0.6J

At energies of 1J and above median cracking and crushing are the dominant cause of fracture as illustrated in fig. 25. The median crack seen in fig. 25. has the characteristic semi-circular shape of these cracks (see p29 - model by Lawn and Fuller [1975]).

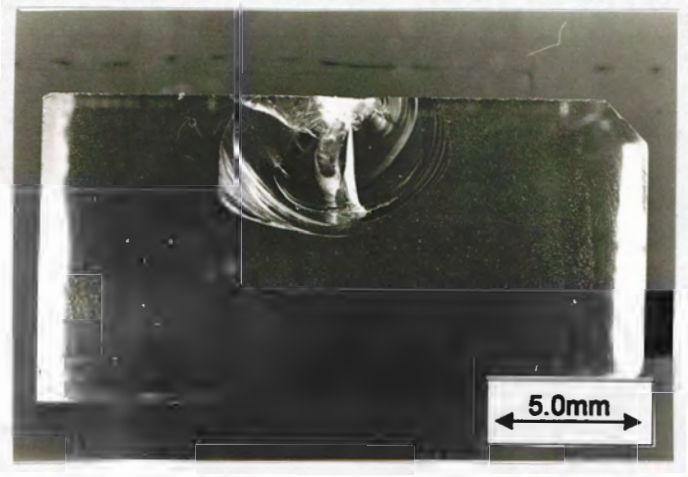

Figure 25. Side view of a glass test block impacted 0.7mm from the front face at an energy of 1.19J

Impact between 0.7mm and 5.3mm from the front face

For fracture to occur when further away from the front face of the test block than 0.7mm the impact energy has to be higher than 1J and as a consequence median cracking dominates the fracture. Fig. 26. shows how a flake forms by bending towards the front face during growth.

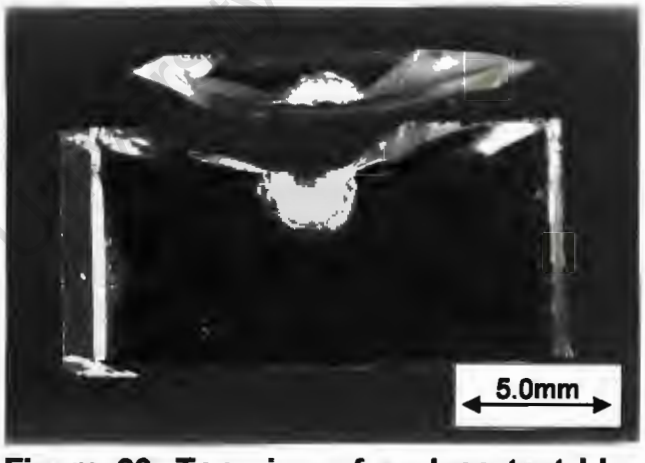

Figure 26. Top view of a glass test block impacted 2.7mm from the front face at an energy of 1.5J

Influence of the notch on the flake

In order to determine if a notch has any effect on the characteristics of the Hertzian failure a diamond pencil was used to make a scratch at 0.7mm from the edge and parallel to the front face of the test block. The presence of the scratch causes no change in shape of the Hertzian edge flake but it does increase the mass (size) of the flake.

Summary of the glass impact results

i. From an impact energy of 0.15J to 0.45J the failure or cracking, occurring at all impact positions from the edge of the test block, is purely Hertzian.

ii. From 0.59J to 0.89J the failure or cracking, occurring at all impact positions from the edge of the test block, is both Hertzian and median.

iii. From 1.04J to 1.63J the failure or cracking, occurring at all impact positions from the edge of the test block, is Hertzian, median and crushing.

iv. Above 0.74J impact energy lateral cracking occurs in combination with the cracking mentioned in ii) and iii).

v. For impact at a distance of 1.7mm to 5.3mm from the front face of the test block an increase in energy causes the crack size to increase. Median cracking is the crack type that causes failure under these conditions.

vi. For impact at a distance of 0.7mm from the front face of the test block, while ***in the pure Hertzian failure range i.e. below 0.89J, the mass (size) of the flake is not dependent on the energy of impact.***

vii. In all the glass impact tests an increase in energy progressively changes the crack type from Hertzian cone cracking to a combination of median and Hertzian cone cracking. It appears that the initiation mechanism changes from that described in fig. 11.(a) to a combination of the cracking in 11.(a & b) for a increase in impact energy.

viii. The presence of a scratch, under the impact site, at a distance 0.7mm from the front face of the test block causes no change in shape of the Hertzian edge flake but it does increase the mass (size) of the flake.

Impact of WC-cermets

All impacting of the WC-cermets was carried out at 0.7mm from the front face as illustrated by fig. 14. The threshold impact energy is the minimum impact energy per blow that will cause a flake to form within 500 impacts while the average mass of the flake is a measure of the average size of the flakes. A discussion will be presented in the following chapter to explain these results and correlate them with the microstructures.

Grade	Binder wt %	Binder Type	WC Grain Size (Om)	Threshold impact energy [J]	Average mass of flake [g]
S6	6	Co	1.3	4.60	0.3819
G6	6	Co	2.3	4.60	0.3112
S10	10	Co	1.2	4.40	0.3041
G10	10	Co	2.0	4.40	0.0166
S15	15	Co	1.6*	4.20	0.0185
G15	15	Co	2.4	3.95	0.0101
V7	6	Ni-Cr	2.0	4.60	0.8628
P15	15	Ni-Cr-Co	2.3	3.95	0.0329

Table 3. Results of impact testing

In order to assist in the interpretation of these results various macroscopic photographs, optical and scanning electron micrographs are presented. The fractography is particularly important for the understanding of the WC-cermet impact results. The scanning electron microscope operating in the back scattered electron mode or secondary electron mode was used to obtain information on the fracture behaviour of the WC-cermet grades.

* Obtained from coercivity measurement

Table 3 lists the grades with the binder percentage, binder type, grain size, threshold impact energy and average flake mass.

The average mass of the flake is a direct indication of its size. The size of the flake formed in each grade is independent of impact energy but it is dependent on the material i.e. binder percentage, grain size, mean free path and contiguity. This impact energy independence occurs because the impact energy remains within the Hertzian range for WC-cermets.

The test rig is not capable of impacting at energies high enough to cause the median cracking seen in the glass. WC-cermets have a higher toughness than glass and thus higher impact energies are required to initiate the types of cracking seen in glass.

Macroscopic examination of flakes

The edge flakes that form in the WC-cermets, form in a Hertzian manner. The shape of the WC-cermet flakes are very similar to the edge flakes that form in the glass where impact is carried out in the energy range that gives rise to Hertzian failure. Fig. 27. shows the shape of a WC-cermet flake. It has a conical type of appearance indicating Hertzian failure. The ring crack and therefore the Hertzian cone intersect the front face of the test block in a similar manner to that seen in glass impact at 0.7mm from the front face. In the figure above as well as later figures the ring crack appears to have a diameter of 2mm to 4mm. This is, however, not the case. The impact head causes damage to the ring crack area as well as the upper portion of the flake when the flake is fractured off the test block. This is caused by the impact head moving to a position slighty below the top surface (impact surface) of the test block.

There are also undulations present on the lower region of the fracture surface. These undulations are symmetrical about a vertical axis that travels through the

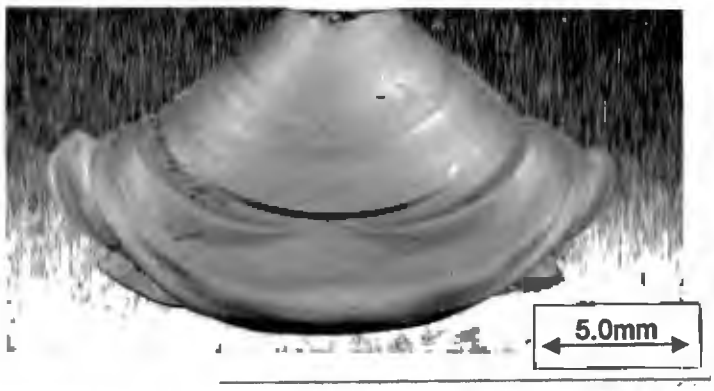

Figure 27. Side view of edge flake produced on the front face of a WC-cermet test block

centre to the test block. The crack front travels in a direction that is perpendicular to the undulations. Near the top of the fracture surface the crack travels diagonally down and into the test block and does not have to undergo a direction change; this gives rise to the smooth fracture surface seen in this region. A little further down the fracture surface, after the crack front has formed the bulb of force or percussion, the symmetrical undulations appear and this can be ascribed to the fact that the crack front is undergoing a change of direction. The reason for this direction change is described by Cotterell, Kamminga and Dickson (1985) and is discussed earlier (see "Impact Testing" - "Edge Flaking" section).

The following figure compares the size of the flakes, produced by impact, of each grade. ***It is important to remember that the size of the flake produced is independent of impact energy but dependent on the grade being impacted.*** For the cobalt grades the size of the flake decreases with increasing binder percentage and increasing grain size.

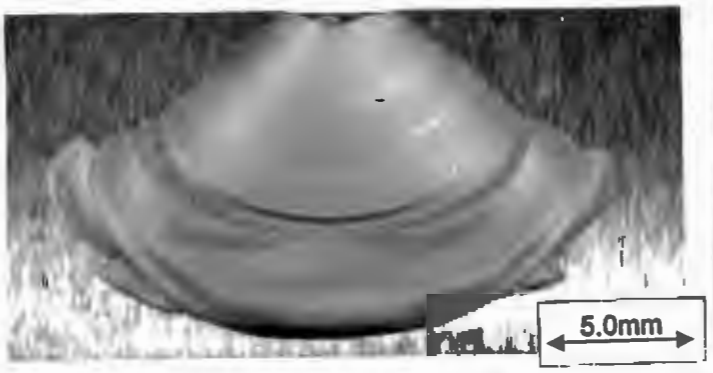

a) S6: 6%Co, 1.3μm Grain Size

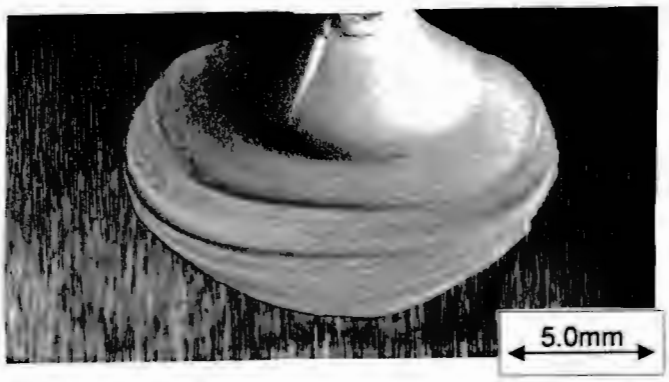

b) G6: 6%Co, 2.3μm Grain Size

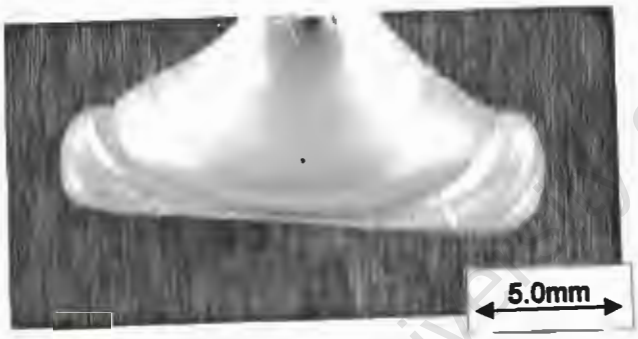

c) S10: 10%Co, 1.2μm Grain Size

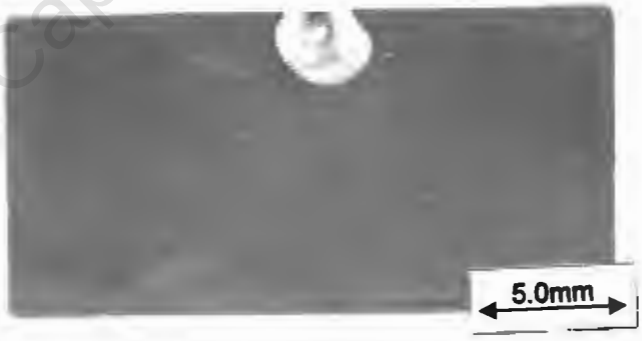

d) G10: 10%Co, 2.0μm Grain Size

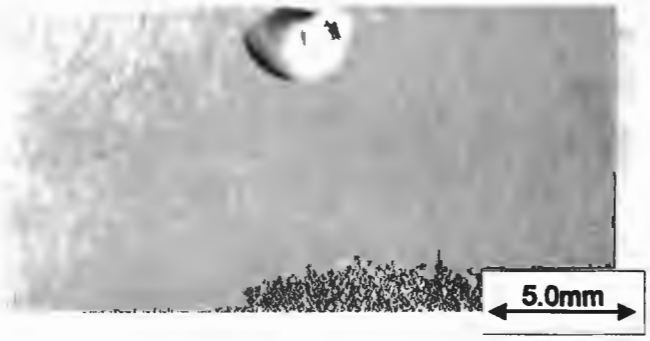

e) S15: 15%Co, 1.6μm Grain Size

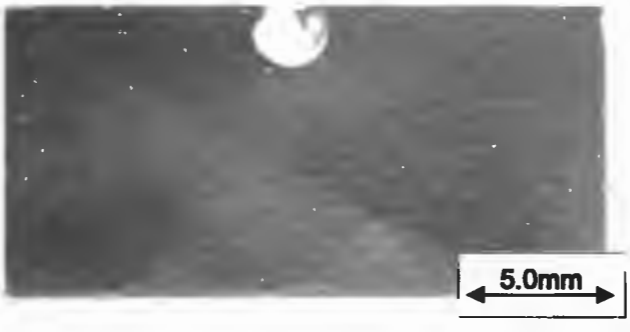

f) G15: 15%Co, 2.4μm Grain Size

g) V7: 6%Ni-Cr, Grain Size 2μm

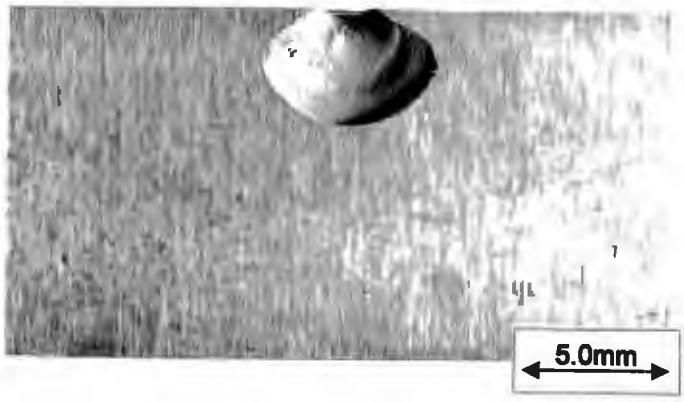

h) P15: 15%Ni-Cr-Co, Grain Size 2.3μm

Figure 28. Macrographs of impacted test blocks

The test block in fig. 28.a) is a S6 grade and shows a slightly larger flake than the G6 grade. The size of the flakes in the G10 grades are much smaller than those of the S10 grade. This large decrease in size of the flakes between S10 and G10 does not follow the trend that is shown between S6 and G6 or S15 and G15, where when going from the S grain size grade to the G grain size grade there is a small decrease in flake size. Also of interest are the extremely large flakes that are produced in the V7 grades as shown in fig. 28.g. The V7 grade is a Ni-Cr binder grade of 6% by wt binder and it forms a much larger flake than the 6% cobalt binder grade. The V7 grade shows hackle marks at the edges of the fracture surface. From back scattered electron studies of the V7 grade a great deal of bifurcation was observed near the crack tips. Fig. 28.h. is a photograph of a 15% Ni-Cr-Co binder grade test block. Comparison with a cobalt binder grade percentage of 15 (Fig. 28.f) shows that the Ni-Cr-Co binder grade forms a larger flake even though the binder percentage is the same.

Comparison of size of flakes

The size of the flakes formed in each of the grades was quantified by weighing the test blocks before and after impacting. The mass of the flakes formed could thus be recorded and the average mass of all the flakes formed in each grade was obtained. A comparison of all the average masses, of the flakes, of the various grades is shown in fig. 29. The average mass of each grade can be taken as a measure of the edge flaking performance for that grade. The smaller the flake size the better the edge flaking performance can be considered to be.

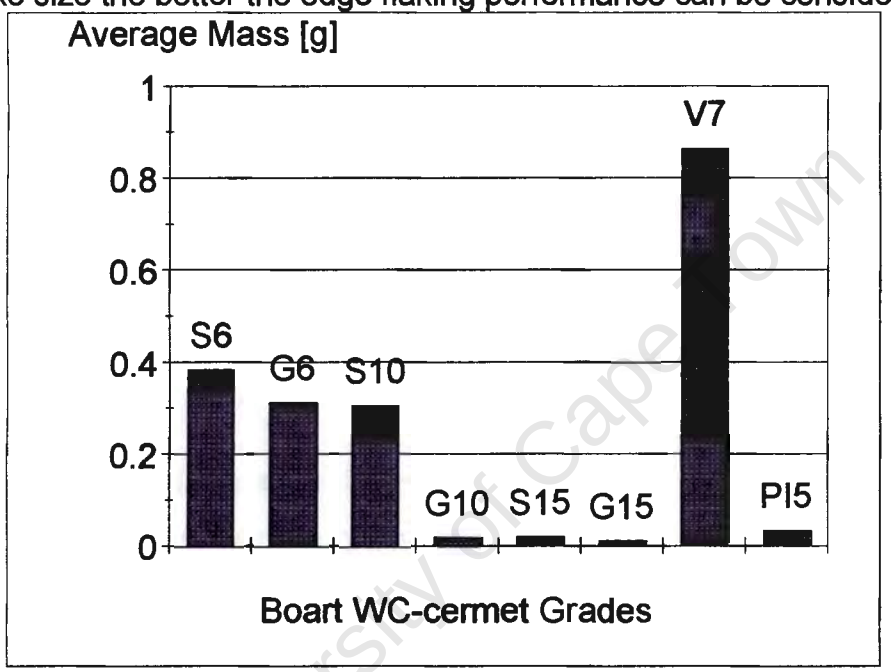

Figure 29. Average mass of the flakes, of all grades

The cobalt grades S6, G6, S10, G10, S15 and G15 (Refer to Table 3 for binder percentage, binder type and grain size of individual grade) show a decrease in flake size with an increase in binder percentage. Grades S6, G6 and S10 have a significantly lower edge flake toughness than G10, S15 and G15. In comparison to all the other grades the 6% Ni-Cr binder grades perform extremely badly with a large average flake mass of over 0.8g. The 15% Ni-Cr-Co grade performs well with a small flake size.

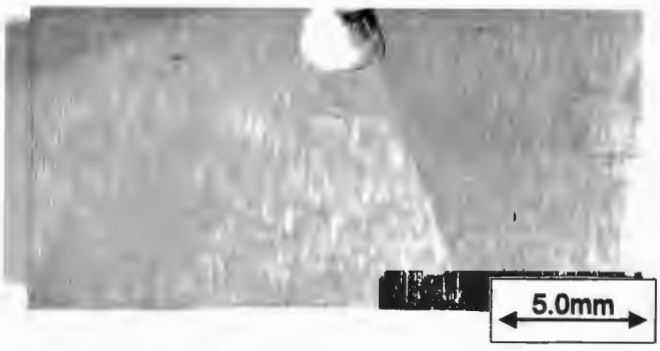

c) G15 Grade: 3.9J impact energy

d) G15 Grade: 4.1J impact energy

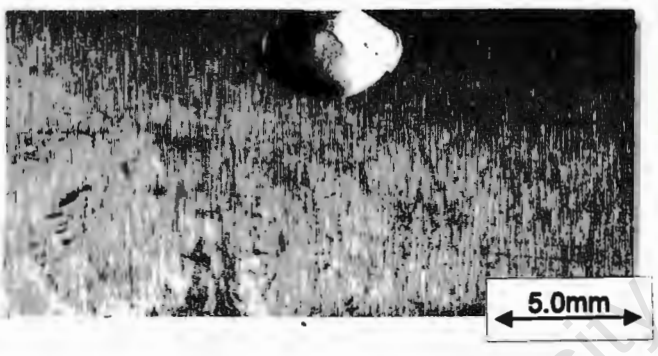

e) P15 Grade: 4.2J impact energy

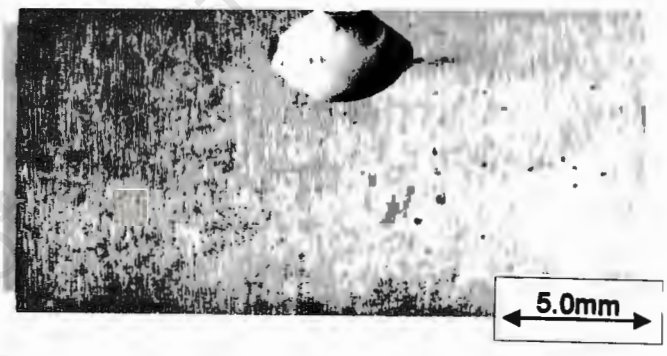

f) P15 Grade: 4.0J impact energy

Figure 33. Comparison of flake size after impact at different energies

Macroscopically the fracture of the WC-cermet grades appear brittle but microscopically, as explained later in the text, ductile and brittle fracture occur to varying degrees in each grade.

Assuming that the speed of the impact head is slow in comparison to the speed of the crack growth the following explanation for the phenomenon of similar flake size under different energies can be considered:

- Grades that show a predominantly brittle mode of fracture will have fast crack growths due to the high elastic energy release during cracking and the lower energy absorption due to lack of plastic work. It is noted by Cotterell et al (1985) that an impact force angled too far towards the front face of a rectangular block will cause the resultant flake to hinge towards the free surface of the block. At the moment of flake formation in the WC-cermet grades the impact head will cause an outwards bending moment of the flake by moving slightly between the flake and the test block. In a grade with a brittle fracture mode, because the fracture occurs fast, the crack will progress far before the flake is hinged off the test block.
- Grades with a more ductile type of fracture have slower crack growth rates due to the high degree of plastic deformation taking place and cracks progress a shorter distance before the flake is hinged off the test block.

Influence of contiguity on flake size

Fig. 34. draws a comparison between the average mass formed in the cobalt grades, the contiguity and the mean-free path of the binder for these grades.

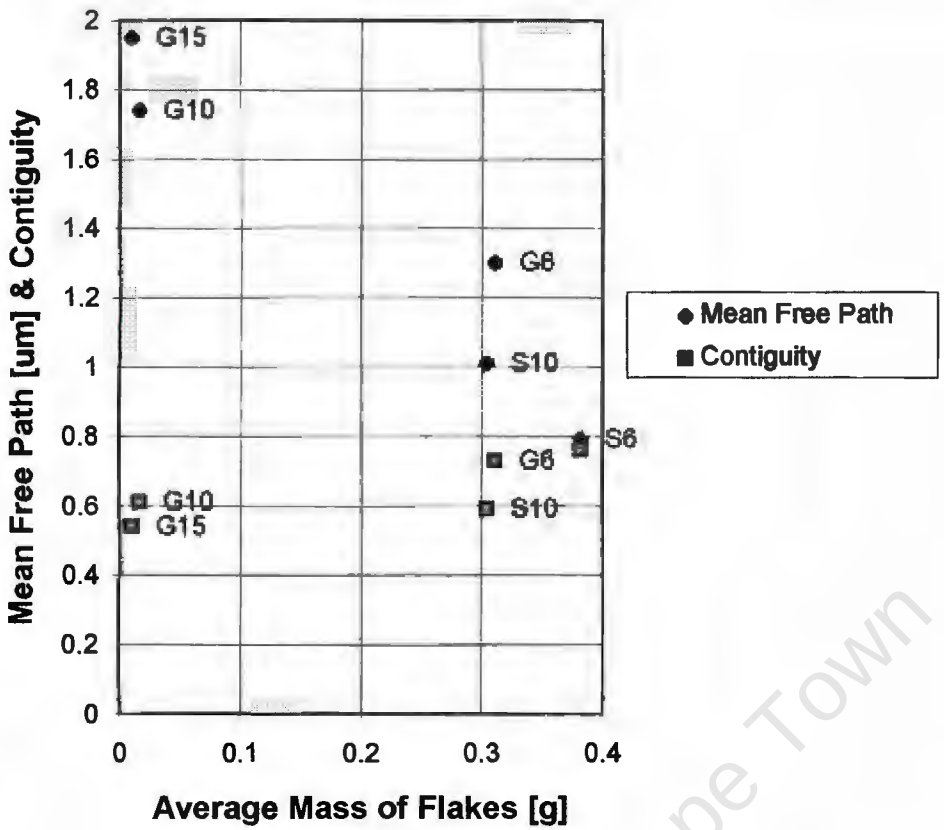

Figure 34. Average mass of the flakes versus mean-free path and contiguity of cobalt grades

The above graph illustrates that the contiguity of the 6% binder grades is higher than the 10% or the 15% binder grades. A high contiguity is consistent with the presence of a continuous WC skeleton. During impact loading, because of the much higher elastic modulus of the WC grains in comparison to the cobalt binder, the stress is transmitted through the WC grains. At the carbide grain contacts there is a high localised stress. Luyckx (1968) reported observing slip lines at the contacts between the carbide grains indicating highly localised stress. This stress can result in the transgranular fracture of the carbide grains. Some fracture of the cobalt binder does occur as well due to the inability of the WC to deform in all slip directions (Rowcliff, Jayaram, Hibbs and Sinclair (1988)).

Influence of mean-free path on flake size

Fischmeister, Schmauder and Sigl (1988) reported that crack propagation in WC-Co is opposed by the plastic stretching of binder ligaments and the fracture energy of the carbides surrounding them. Godse and Gurland (1988) state that the mean-free path in the binder phase exerts a large influence on the mechanical properties of hardmetals. Rice and Johnson (1970) predicted a zone of intense strain of size D in front of the crack tip. This zone of stress, according to them, should envelop a characteristic microstructural dimension l* before ductile growth can commence i.e. D=l*. This dimension D was used by Godse and Gurland (1988) to present a model that predicts that the initiation of crack growth occurs when the region D of intense strain envelops the characteristic microstructural distance λ (mean-free path), or alternatively when the strain at a distance λ from the crack tip reaches a critical value. They go further to say that an increase in toughness with an increase in λ is a consequence of the fact that the region D has to spread over a greater distance before crack growth can occur.

This means that the larger the mean-free path (λ) the more energy is needed to propagate a crack through the cermet. A large mean-free path results in a shorter critical crack length and thus a smaller flake.

Fig. 34. shows a substantial increase in the binder mean-free path between the S10 and G10 grade. This increase in mean-free path is the reason for the large decrease in flake size between the S10 grade and the G10 grade. It would appear that the contiguity has less influence on the flake size because there is little variation in the contiguity between the S10 and the G10 grade.

The fact that mean-free path has more influence than the contiguity explains the decrease in flake size of the G grades as opposed to the S grades as seen in the fig. 29., 30. and 32.

The G grades have a larger grain size than the S grades and therefore have a higher mean-free path resulting in more ductile deformation during crack growth.

An increase in the mean-free path also results in less plastic constraint on the binder, stress levels in the carbide grains cannot be raised sufficiently to cause these grains to fracture.

Correlation of crack growth paths and related fracture surfaces with flake mass (size)

The back scattered electron (BSE) technique was used to study the crack growth paths in the cermets. Fig. 35. is a set of BSE micrographs of crack growth paths in the cobalt grades. All the BSE images are cross-sections cut through the impact site. They were diamond lap polished to 0.25μm and left unetched, to preserve the binder in the crack paths.

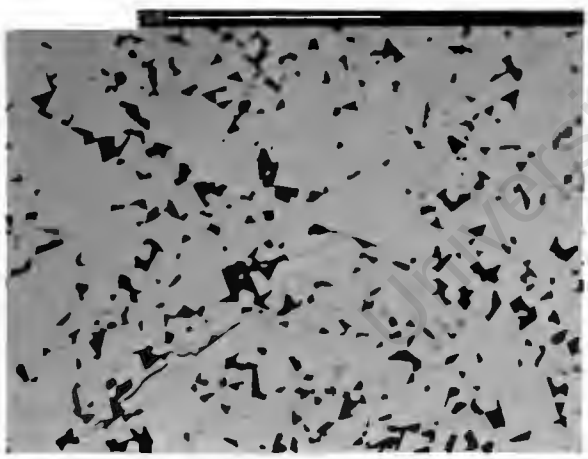

35.a) S6: 6%Co, 1.3μm Grain Size

35.b) G6: 6%Co, 2.3μm Grain Size

35.c) S10: 10%Co, 1.2μm Grain Size

35.d) G10: 10%Co, 2.0μm Grain Size

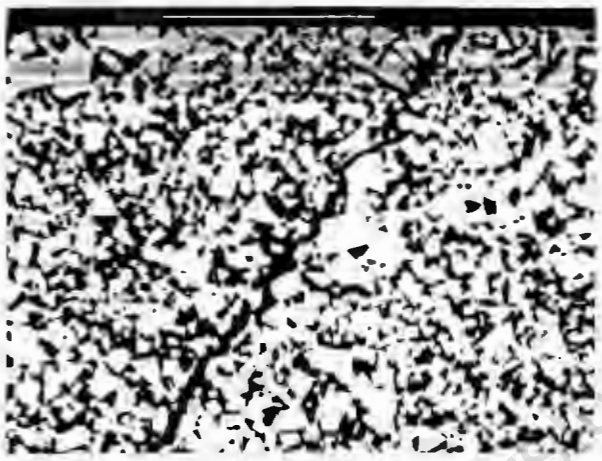

35.e) S15: 15%Co, 1.6μm Grain Size

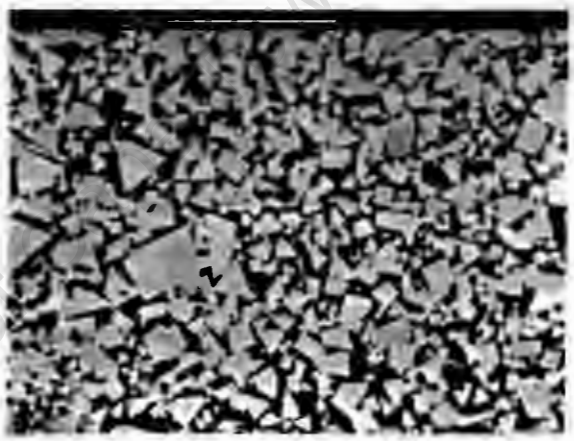

35.f) G15: 15%Co, 2.4μm Grain Size

Figure 35. Back scattered electron images of crack paths in cobalt grades

As the binder percentage increases from 6 to 15 (a to f) the amount of transgranular fracture becomes less. In a comparison of the S10 and G10 grades (c & d) the amount of transgranular fracture appears significantly less in the G10 grades, although this method of judgement is rather subjective.

To obtain a better understanding of the fracture mechanisms occurring in the grades their fracture surfaces were studied using the secondary electron technique. The fractures observed in the cobalt grades are shown in fig. 36.

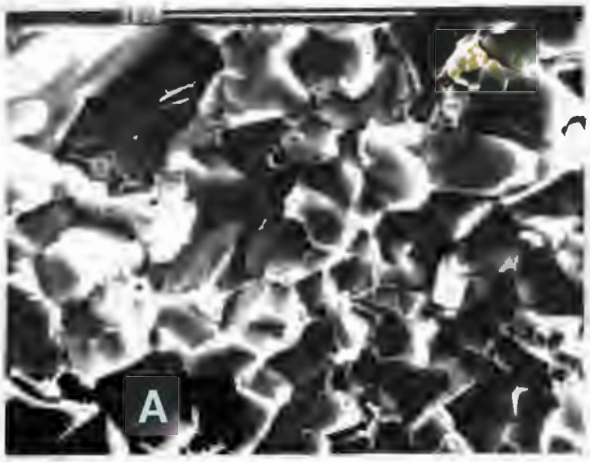

36.a) S6: 6%Co, 1.3μm Grain Size

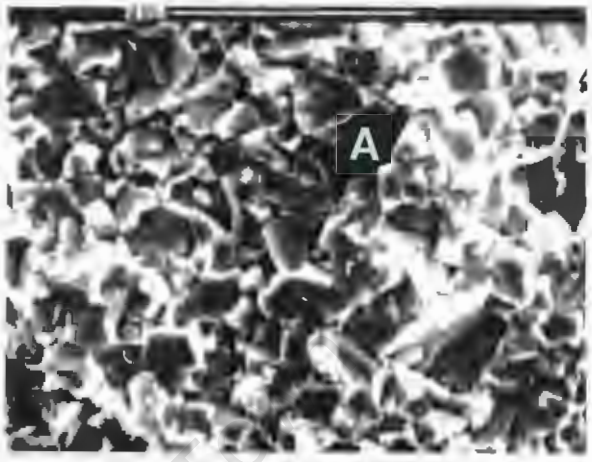

36.b) G6: 6%Co, 2.3μm Grain Size

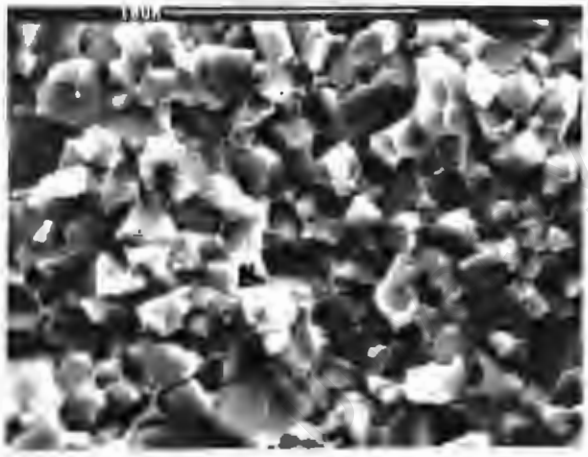

36.c) S10: 10%Co, 1.2μm Grain Size

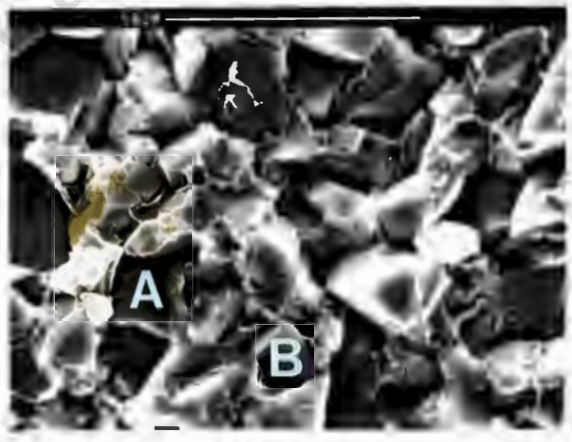

36.d) G10: 10%Co, 2.0μm Grain Size

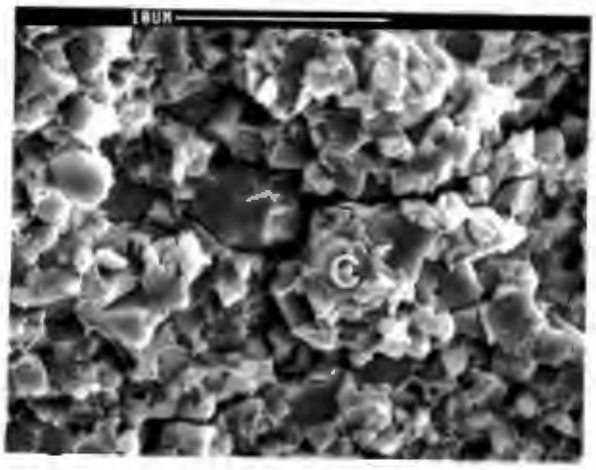

36.e) S15: 15%Co, 1.6μm Grain Size

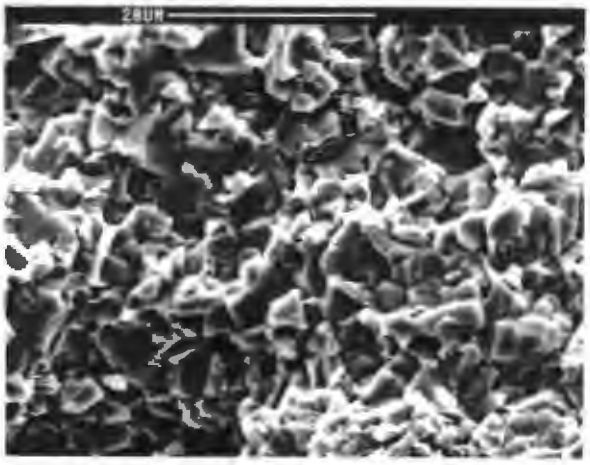

36.f) G15: 15%Co, 2.4μm Grain Size

Figure 36. Secondary electron images of fracture surfaces in cobalt grades

As the binder percentages increase the fracture surfaces change character from that of brittle fracture to that of relatively ductile fracture. In micrograph 36.a) a 6% cobalt binder grade with a small grain size of around 1.3μm (S6) is illustrated. The fracture surface shows evidence of brittle transgranular fracture (a cluster of fractured WC grains is marked at A). The carbide grains are fractured and this leaves behind very little binder residue on the surfaces of the grains. In this micrograph the binder can be seen as the lighter film sandwiched between the grains and only in a few places is it left behind on the surface of the carbide grains.

The fracture surface of a 6% binder grade with the larger grain size of 2.3μm (G6) is illustrated in 36.b). This fracture surface also has a brittle appearance with a high degree of the cleavage of the carbides and only a small amount of binder is left behind on these grains (a cluster of fractured WC grains is marked at A).

Micrograph 36.c) illustrates the fracture surface of the smaller grain size (1.2μ m) 10% cobalt binder grade (S10). More binder is in evidence on the fracture

surface of this higher cobalt percentage grade but there is also a high degree of cleavage of the carbide grains.

In micrograph 36.d) the G10 grade shows a large degree of ductile fracture as opposed to the previous three illustrated fracture surfaces. The fracture surface in this micrograph is highly faceted with a great deal of binder left behind on the surfaces of the grains indicating intergranular fracture (one of the faceted areas is marked at B). The dimpling of the binder that is left behind on the carbide grains is as a result of ductile ligament formation and rupture during the separation of the carbide grains. Fischmeister et al (1988) reported that deep dimples develop during fracture across a ligament while shallow dimples characterise crack paths parallel and close to the binder-carbide interface. The high amount of ductility illustrated in this micrograph results in a large degree of plastic work occurring during crack growth in this grade and this explains its resistance to edge flaking. Only a small degree of carbide cleavage can be seen in this grade (one of these areas is marked at A).

The flake fractography of the small grain sized (1.6μm) 15% binder grade (S15) is illustrated in micrograph 36. e). This fracture surface also shows a high degree of ductile fracture. It has a faceted appearance much binder is in evidence on the WC grains. Large areas of binder can be seen in this micrograph (one area marked at C) and they appear as lighter areas with a random tiled type of texture. Dimpling can be seen as well. In this micrograph a secondary crack can be seen travelling from the upper right-hand corner to the bottom left-hand corner. The ductile mode of fracture seen in this grade gives rise to good edge flake resistance.

The fracture surface of the G15 grade, which has a grain size of 2.4μm and a binder percentage of 15, is illustrated in micrograph 36.f) and it also shows a high degree of ductile failure (one area marked at C). Dimple regions are less in evidence on this fracture surface not due to less ductile behaviour but

because there is much less plastic constraint of the thick binder regions and thus the dimple regions form less often. The large areas of binder show a similar random tiled texture as described in the previous micrograph 36.e). Even in these cobalt grades, with a higher mean-free path (G10, S15, G15), a small degree of transgranular fracture does occur but the overwhelming type of fracture is ductile, giving rise to good edge flake resistance.

The Ni-Cr and the Ni-Cr-Co binder grades show a distinctly inferior edge flaking performance in comparison to their equivalent (same binder content) pure cobalt binder grades. It is reported by Eun, Kim and Yoon (1984) that substitution of cobalt by nickel in WC-cermets does not greatly affect the transverse rupture strength if the grain size remains constant. The addition of chromium carbide (Cr_3C_2), however, has a much more noticeable effect. Chromium is a WC grain growth inhibitor. Human, Northrop, Luyckx and James (1991) observed that increasing levels of chromium resulted in a finer microstructure and therefore higher hardness and lower toughness values. A finer microstructure will result in a small binder mean-free path. Mean free path has a very large effect on the edge flaking performance of the cobalt binder grades. Human et al (1991) also reported that the transverse rupture strength of Ni-Cr and Ni-Cr-Mo alloys is between 6% and 16% lower than that for the WC-Co alloys. This was considered to be partly due to the fact that the nickel-based binder alloys manufactured by Boart had calcium sulphide/sulphate inclusions up to 200μm in size as a result of contamination during preparation of the alloys.

Tracey (1992) suggests that the wetting of Cr_3C_2 by nickel is poor. The wetting of Cr_3C_2 is poor below 1200°C due to chromium oxide present on the surface inhibiting wetting but it improves to a degree above 1200°C when the chromium oxide is reduced. This poor wetting of the Cr_3C_2 results in large nickel pools being formed in the structure which has an adverse effect on the mechanical properties of the grades with Cr_3C_2 additions.

Tracey (1992) also stated that the control of carbon, to avoid eta-phase (Co_3W_3C) or graphite formation, is necessary to develop optimum properties. For WC-Ni the carbon level should be around 6.05wt % but according to Tracey there is controversy over whether eta-phase tended to form more readily with nickel based binders.

Back scattered electron images of the V7 grade (94% WC, 5.63% Ni and 0.37% Cr) are illustrated in fig. 37.a) and 37. b)

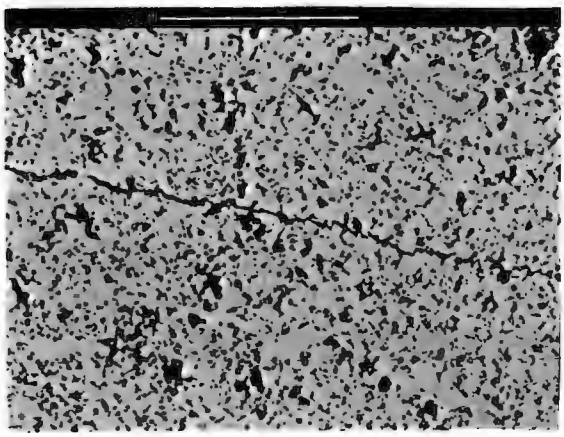

37.a) V7: 6%Ni-Cr, 2.0μm Grain Size

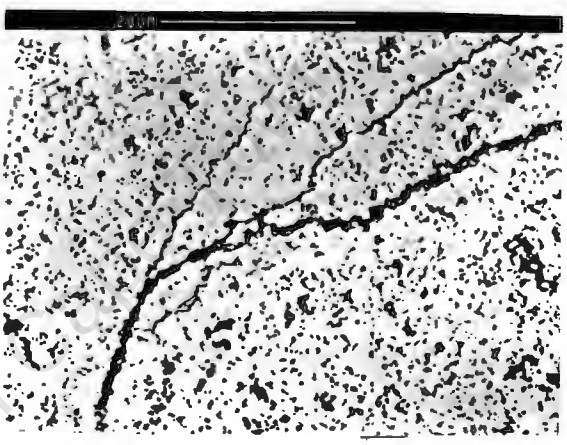

37.b) V7: 6%Ni-Cr, 2.0μm Grain Size

Figure 37. Back scattered electron images of V7 grade

In the above micrographs the microstructure of the V7 grade shows a large degree of grain refinement brought about by the chromium additions. There are very few large grains visible and this suggests that the grain size distribution is much narrower than that of the cobalt binder grades. There are also a great deal of binder pools present in this grade. Both the binder pools and the fine grain structure contribute to decreasing the mean-free path in a cermet and this increases the likelihood of brittle failure. A large amount of crack bifurcation can was also observed in this grade as illustrated in fig. 37.b).

Investigation of the fracture surfaces of the V7 reveals a brittle fracture mechanism. The fracture surface of the V7 grade is illustrated in fig. 38.

Figure 38. Fracture surface of V7 grade

In the above micrograph there is a high degree of carbide grain cleavage and very little binder left behind on the surface of the grains. The flat grains are those that have been fractured by transgranular cleavage. This indicates that brittle failure has occurred and would explain the poor performance of this grade in the edge flake testing.

The P15 grade (85% WC, 7.2% Ni, 6.2% Co, 1.6% Cr) also has a poor edge flaking performance. A back scattered electron image of this grade is shown in fig. 39.

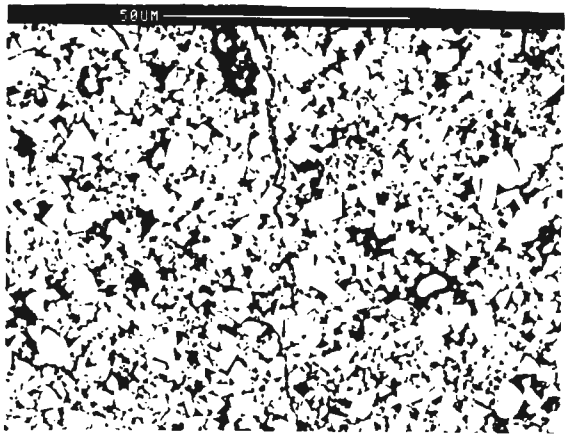

P15: 15%Ni-Cr-Co, Grain Size 2.3μm

Figure 39. Back scattered electron image of P15 grade

This grade has a less refined grain structure than the V7 grade illustrated in fig. 37. There are some very large grains present in the P15 grade as can be seen from fig. 39. Human et al (1991) believes that the nickel forms an oxide skin during sintering which is further stabilised by additions of chromium and this inhibits diffusion of tungsten and carbon into the nickel binder requiring a higher sintering temperature. The larger grains have been caused by grain growth in the P15 cermet due to higher sintering temperatures.

The P15 grade shows large binder pools, seen as dark areas in fig. 39., and this would serve to lessen the average mean-free path of the binder and encourage brittle failure. The crack in fig. 39. undergoes a high degree of transgranular fracture.

The fracture surface of the P15 grade is illustrated in fig. 40.

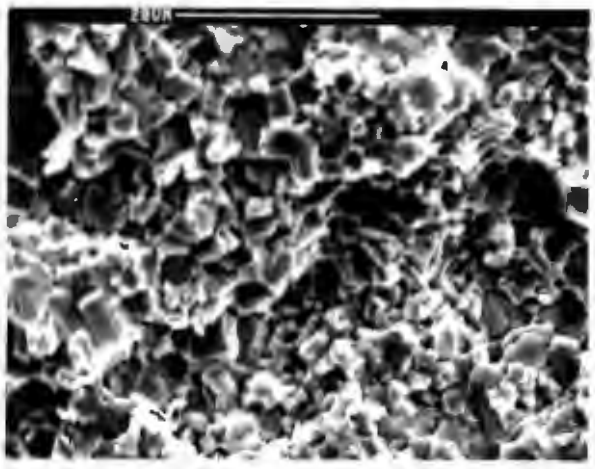

Figure 40. Fracture surface of P15 grade

On the fracture surface of the P15 grade it is hard to distinguish the difference between the binder and the carbide grains. The carbide grains appear to be grey in colour and flat in shape. The flat appearance is because they have been fractured through. The less uniform areas are large binder areas which have undergone ductile failure. This fracture surface shows a combination of ductile and brittle failure. This explains why the average mass of the flakes formed in this grade is larger than the G10, S15, and G15 grade (which show a high degree of ductile failure) but not as large as the V7, S6 and S10 grade (which shows a high degree of brittle failure).

Influence of carbon balance on flake size

The elimination of eta phase is important to obtain good mechanical properties in WC-Co cermets. Eta phase has the chemical composition Co_3W_3C and is harder and more brittle than WC. This phase forms as a result of an insufficiency of carbon to form WC being present in the sintered component. The presence of eta phase can quickly be detected by measuring the magnetic saturation of the sintered component or by etching a polished microstructure for 30 seconds in Murkami's reagent. A low magnetic saturation indicates lack of carbon and a high magnetic saturation indicates the presence of free carbon.

The microstructures of all the grades tested were free of eta phase except for the P15 grade. The P15 grade has a magnetic saturation of 68% of theoretical stoichiometry; small areas of eta phase are visible in the microstructure. The presence of eta phase in this grade causes it to perform in a more brittle manner during edge flake testing. This is a further reason the grade to has a lower edge flake toughness than the other 15% binder grades.

Average flake mass compared to other microstructural properties

Binder content:

A comparison of flake mass (edge flaking performance) and binder percentage is made in fig. 41.

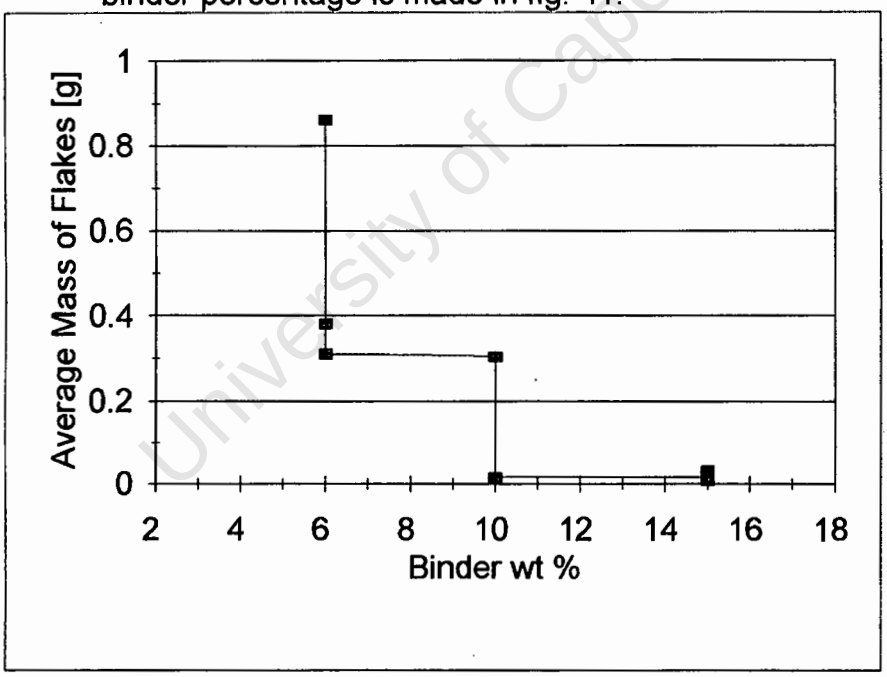

Figure 41. Average mass of flakes versus binder wt percentage

The binder % is inversely proportional to the flake mass and thus directly proportional to the edge flaking performance of the WC-cermet. There are exceptions to this trend and a detailed discussion of the factors behind this are given in the previous sections. These factors include a

lowering of the contiguity and an increase of mean free path, with an increase of binder percentage.

Grain size:

Before a comparison of grain size and average mass is presented the relationship between the grain size and coercivity is given. The S15 grade that was tested is not a standard industrial grade and was specially produced for this study. The grain size of the S15 was determined from its coercivity.

Coercivity is a very important control method for the manufacture of WC-cermets and is determined according to ISO 3326. Assuming the carbon balance is correct the coercivity of a sintered cemented WC-Co is inversely proportional to the WC grain size. For each binder percentage a decrease in coercivity correlates with an increase in grain size. This phenomenon is illustrated in fig. 42. for the S6 & G6 and the S10 & G10 grades.

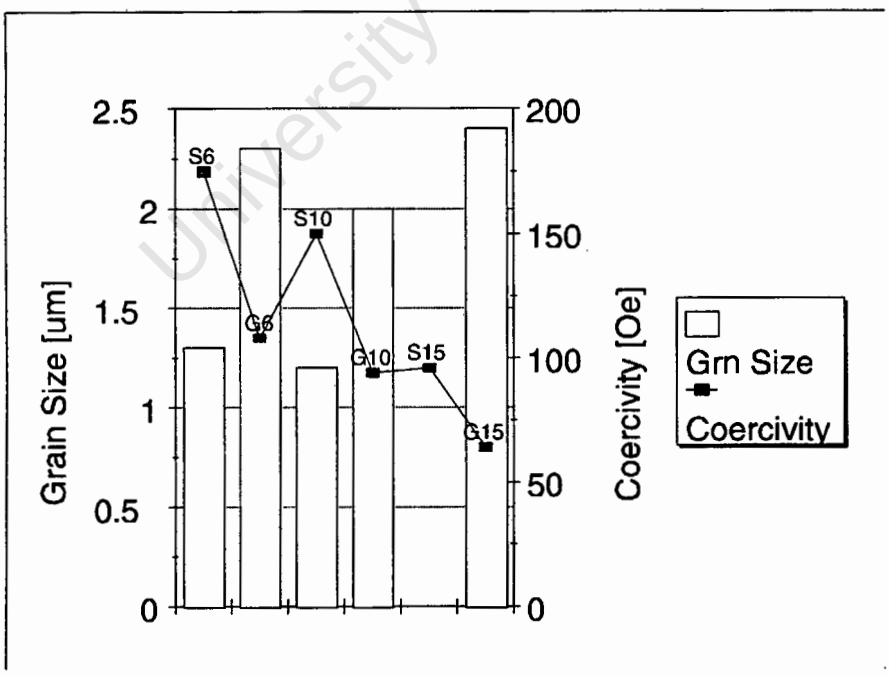

Figure 42. Grain size and coercivity for the cobalt grades

Only the cobalt grades are shown in fig. 42. since coercivity is a magnetic property and the nickel and chromium in the V7 and P15 grades affect their coercivity values.

For the cobalt grades and a *given* binder %:

$$d_S/d_G = 0.6 = (1/Cy_S)/(1/Cy_G) = Cy_G/Cy_S$$

where:

d_S = WC grain size of the S grade

d_G = WC grain size of the G grade

Cy_S = Coercivity of the S grade

Cy_G = Coercivity of the G grade

$$\therefore d_S = (Cy_G x d_G)/Cy_S$$

For the S15 grade:

$$d_{S15} = (Cy_{G15} x d_{G15})/Cy_{S15}$$
$$= (64Oe \times 2.4\mu m)/96Oe$$
$$= 1.6\ \mu m$$

After obtaining the grain size estimate of the S15 grade it was included in the following graph:

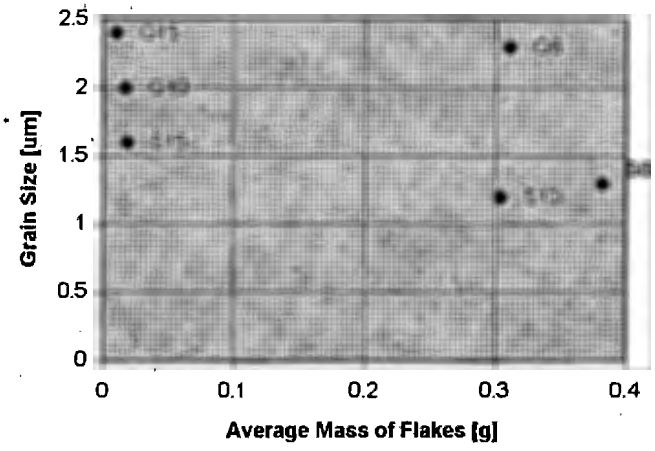

Figure 43. Average mass of the flakes versus grain size for the cobalt grades

The above graph shows that for each binder content (e.g. S6 and G6, S10 and G10, S15 and G15) as the grain size increases the flake size decreases. An increased grain size for a fixed binder content causes an increase in mean-free path of the binder around the carbide grains and this in turn will decrease the length of crack growth.

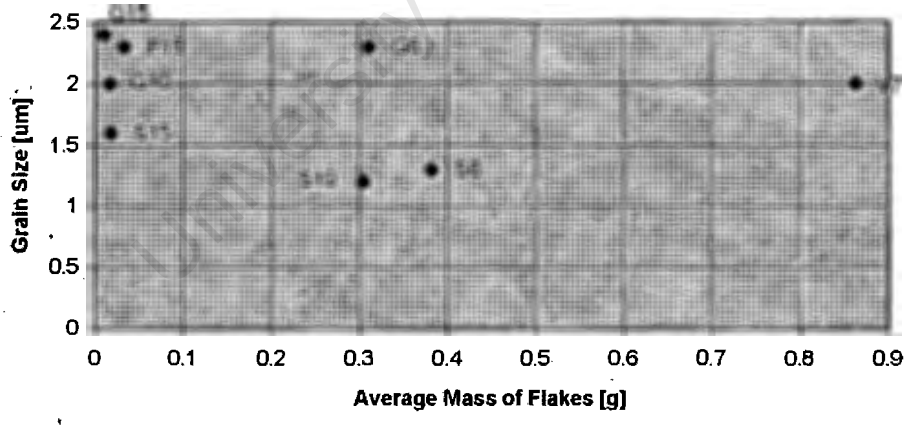

Figure 44. Average mass of flakes versus grain size of all grades

Fig. 44. compares the average mass and grain size of the cobalt grades and the V7 and P15 grades . The average mass of the flakes for the V7 and P15 grades does not follow the same trend, with grain size, as the cobalt grades do.

Average flake mass compared to some mechanical properties

Hardness:

A standard hardness test of the WC-cermets is the Vickers indentation method according to ISO 3878. A low indentation load of 29.4N is used in order to avoid causing excessively long cracks in the corners of the indentation. The presence of these cracks may result in false readings in the higher hardness grades.

WC-cermets obtain their high hardness from the hard brittle carbide phase and the plastic constraint of the binder. The binder phase is considered to be continuous, but there is apparently disagreement about the degree of contiguity of the carbide phase. Lee and Gurland (1978) refer to electron microscopic studies that record deformation by slip in the WC particles which is given as a reason for bulk deformation of the cermet to occur where there is a continuous carbide skeleton. Another school of thought assumes carbide particles are embedded in a continuous binder phase with thin cobalt films separating the individual carbide grains. For this model, the binder phase constraint will play a dominant role in the plastic deformation of WC-cermets.

The hardness of a cermet will decrease dramatically with increasing binder content as illustrated in fig. 45.

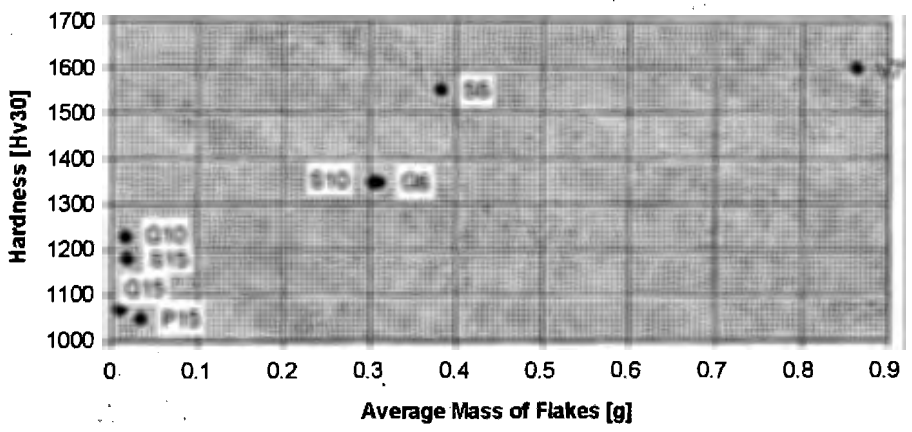

Figure 45. Average mass of flakes and hardness

The average size of the edge flakes decreases and thus edge flaking performance increases as the binder percentage increases and this generally correlates with the drop in bulk hardness of these cermets. The hardness of these cermets gives only an indication of their edge flaking performance and does not predict this property accurately. There are many deviations in the trend shown by hardness in comparison to the trend shown by edge flaking performance, notably for the V7 and P15 grades. The reasons for this have already been discussed in detail and are related to mean free path (binder constraint), contiguity and carbon balance.

Fracture toughness:

The fracture toughness of a WC-cermet is increased with increasing binder percentage and increasing grain size. Both increased binder percentage and increased grain size increase the mean-free path of the binder. With a higher mean-free path of the binder the cracks that grow in the cermet undergo a higher plastic deformation and this absorbs more energy thus improving their fracture toughness. A comparison of fracture toughness and the average mass of the flakes is given in fig. 46.

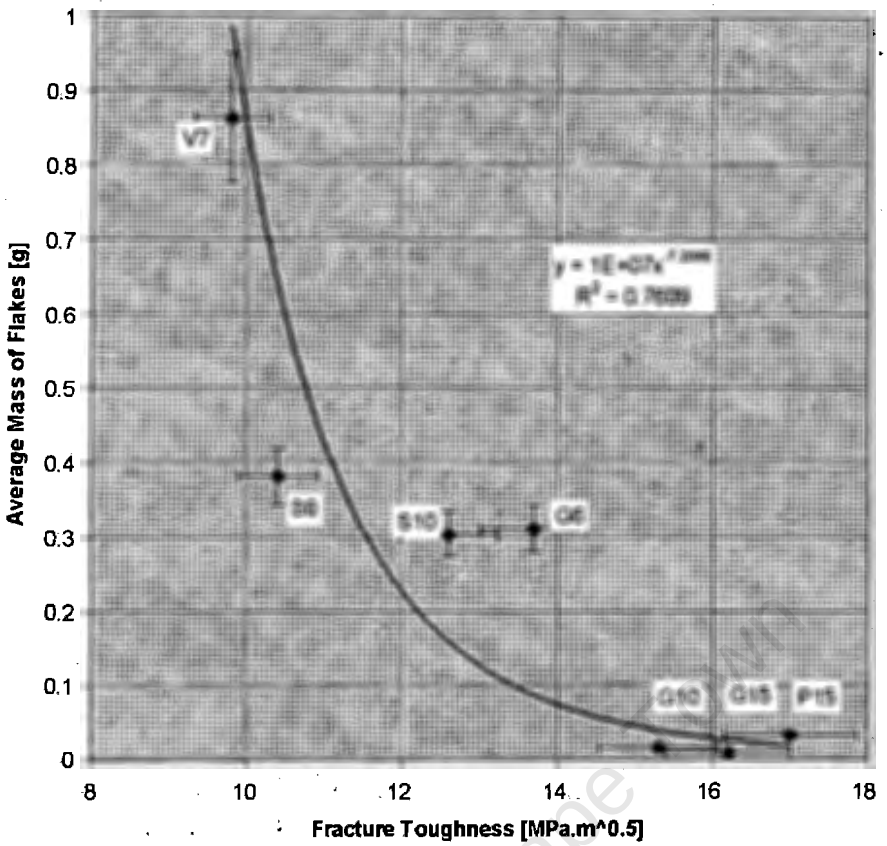

Figure 46. Fracture toughness versus average mass of flakes

The mass of the impact flakes is inversely proportional to the fracture toughness. There is an increase in fracture toughness between the S10 and G10 corresponding to a sharp drop in flake mass and this is as a result of the increased binder mean-free path of the G10 grade. The fracture toughness and edge flaking performance are a function of the binder mean-free path and it would therefore be reasonable to assume that edge flaking performance can predict fracture toughness. It is, however, not necessarily the case as is shown by the graph in the above figure. An exponential curve was fitted to the data points. It has the form:

$$\text{Flake Mass} = k.K_{1C}^{-n}$$

Flake mass and K_{1C} error estimates are also included on the graph.

The low R^2 value indicates that the data does not fit the curve very well. The S6, G6 and S10 grades fall outside the curve even after taking into account their error estimates. Other relationships (power, logarithmic, linear and second order polynomial) do not give an acceptable fit to the data points either. Edge flaking performance does thus *not* appear to be a more practical way to determine fracture toughness.

Fatigue:

Fry and Garrett (1988) tested the S6, S10, G10 and G15 grades under fatigue conditions. They reported that the larger grain sizes and higher binder percentage grades had a lower crack growth rate under fatigue conditions, similar to what was seen for the fracture toughness values.

The edge flake testing did not appear to give rise to progressive crack formation as seen in fatigue cracking. Fracture appeared, however, to occur by firstly going through an initiation stage followed by catastrophic failure without showing the stable crack growth regime seen in fatigue cracking.

Compressive strength and Young's modulus:

The comparisons of the average flake mass with compressive strength and Young's modulus are made in fig. 47. and 48.

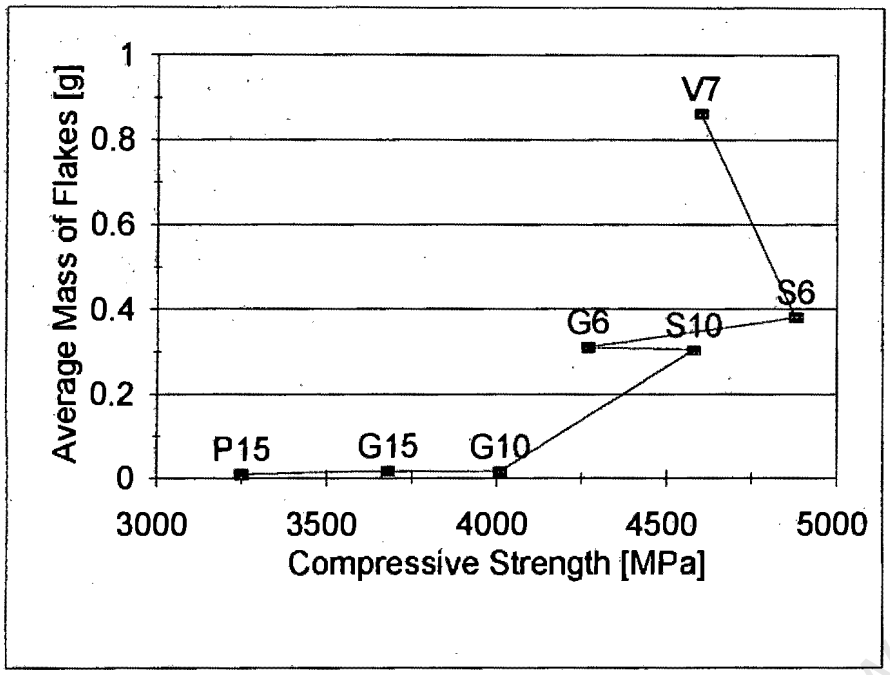

Figure 47. Average mass of flakes versus compressive strength

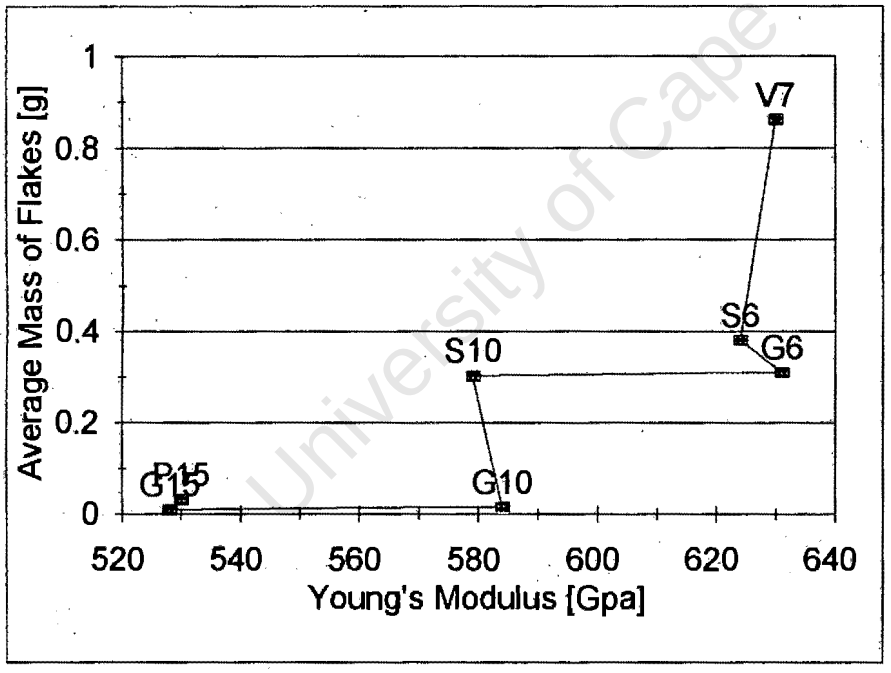

Figure 48. Average mass of flakes versus Young's modulus

Comparison of average flake mass and threshold impact energy

For different grades a characteristic minimum energy is necessary to cause a flake to form. Some grades have a very similar minimum impact energy and

due to experimental error and the normal statistical variation of the brittle materials they could not be ranked against each other.

The impact energy versus the average mass of the flakes is illustrated in fig. 49. Each point on fig. 49. represents a different grade. The points correspond to the minimum energy required to form a flake in each grade and the average mass of the flake formed in each grade.

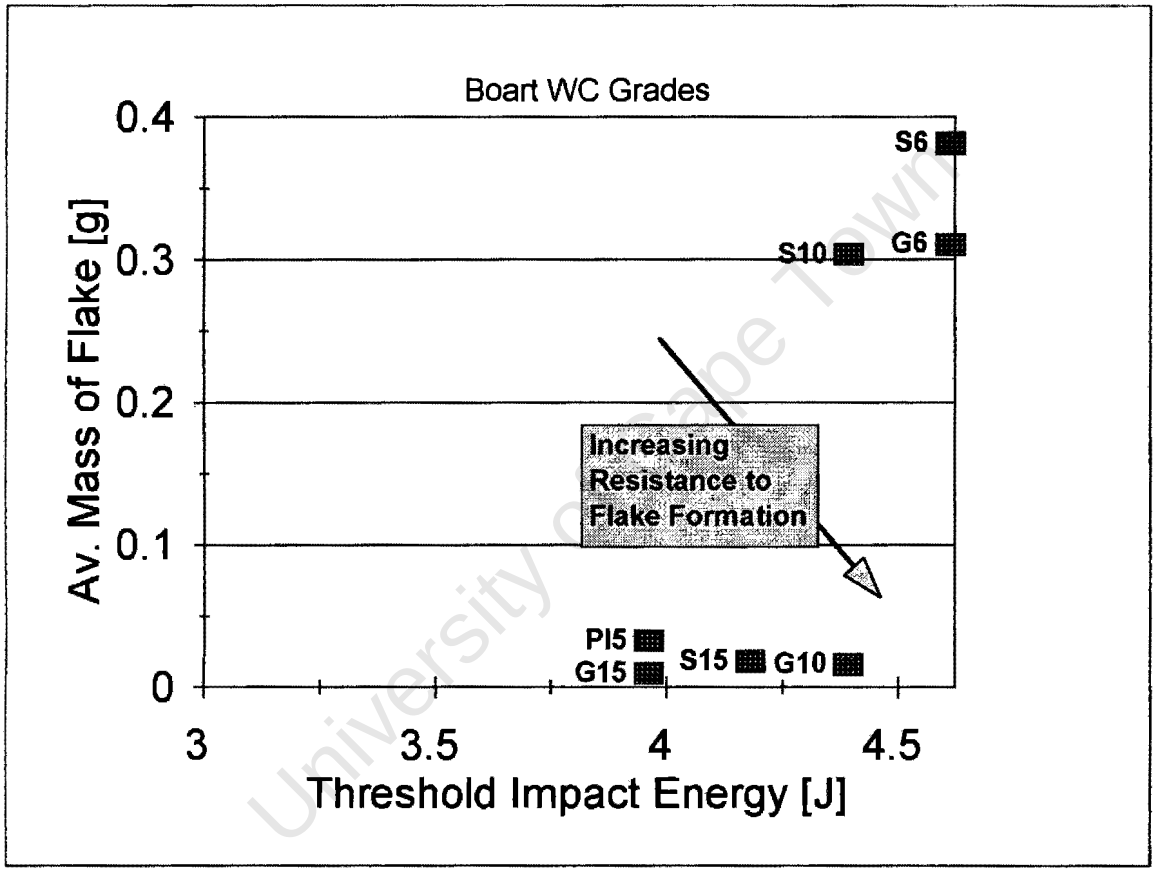

Figure 49. Threshold impact energy versus average mass of the flakes for all grades

Grades P15, G15, S15 and G10 form the smallest flakes during impact and thus can be considered to be more flake resistant than the S10, G6 and S6 grades. While the S6 and G6 grades take a higher energy to form a flake, when they do the size of the flake is large. The V7 grade flakes at a similar energy to the G6 and S6 but forms an extremely large flake and therefore is not illustrated on the

above graph. The G10 grade while forming a small flake also requires a higher energy to form a flake than the P15, G15 or S15 grades and thus to performs the best in this testing. G10 has the highest edge flake toughness.

The lower binder grades require a higher energy to initiate the flake. This phenomenon can be ascribed to a combination of two factors:

- The grades with a low binder percent and thus a low mean-free path have a higher triaxial stress system set up when the carbides are pulled apart during fracture. The binder is plastically constrained by the WC grains. Both Fischmeister et al (1988) and Spiegler, Schmauder and Exner (1992) described triaxial stress systems occurring in the binder after performing finite element analysis on WC-cermets. With more plastic constraint higher stress is needed to fracture the binder. Even in grades with a low mean-free path of binder some binder has to be fractured and this will influence the stress levels needed to initiate fracture.

- Although WC grains absorb far less energy during cleavage than the binder does during ductile ligament rupture they may require a higher stress to initiate fracture in them than the softer binder. This probably has the greatest influence due to the higher amount of transgranular fracture that occurs in the low mean-free path grades.

Conclusion

From the results of the impact testing in glass and WC-cermets as well as the study of the microstructural and macrostructural features of the WC-cermets a number of conclusions can be drawn.

Dynamic loading does appear to be markedly different to static loading in at least one particular aspect. The dynamic loading testing carried out, by the author of this thesis, shows a strong material dependency for the size of the flake; according to Almond and McCormick (1986) the size of the flakes formed during static indentation depends only on the distances of the loading point from the edge and is relatively independent of the material.

After modelling the cracking, by means of impacting glass, it can be concluded that the failure that occurs while impacting at 0.7mm from the edge of the WC-cermet test block is Hertzian. There also appears to be no influence on the shape of this flake when a notch is introduced. The notch serves only to increase the size of the flake.

For impact of the WC-cermet test blocks the following has been established:

- An increase in binder content causes the flakes to become smaller.

- An increase in grain size, for a given binder content, leads to a decrease in flake size because the binder mean-free path increases.

- The Ni-Cr and Ni-Cr-Co grades do not perform as well in the testing as their equivalent cobalt grades.

References

Auerbach F. (1891): Annual of Physical Chemistry, 43 61

Almond E. A. and McCormick N.J. (1986): Letters to Nature, 321 p53-55

Ball A. and McKenzie H.W. (1994): J. de Physique IV 4 Colloque C8 p783-788

Bernard R. (1958): Jernkontorets Ann., 147 p22

Cooper R., Manktelow S.A. and Wong F. (1988): Mat. Sci. and Eng., A105/106 p269-273

Cotterell B., Kamminga J. and Dickson F.P. (1985): Intl J. of Fracture, 29 p205-221

Doeg H.H. (1960): J. of the S.A.I.M.M., p663-679

Ekemar S., Lindholm L. and Hartzell T. (1982): 10th Plansee Seminar, Reutte, R&HM March 1982 p37-40

Erdogan F. and Sih G. C. (1963): J. Basic Eng., Trans A.I.M.E. 85D p519

Eun K.Y., Kim D.Y. and Yoon D.N. (1984): Powder Met., 27 No.2 p112-114

Exner H.E. (1979): Inl Metals Rev., 243 No4 p149-173

Exner H.E. and Gurland J. (1970): Powder Met., 13 No25 p 13-31

Fischer-Cripps A.C. and Collins R.E. (1994): J. of Mat. Sci., 29 p2216-2230

Fischmeister, H.F. Schmauder S. and Sigl L.S. (1988): Mat. Sci. and Eng., A105/106 p305-311

Frank F.C. and Lawn B.R. (1967): Proc. of the Roy. Soc., 299A p291-306

French D. N. (1969): J. Amer. Ceram. Soc., 52 p267 & 271

Friederich K.M. (1983): Metal Sci., 17 p456-458

Fry P.R. and Garrett G.G. (1988): J. of Mat. Sci., 23 p2325-2338

Godse R. and Gurland J. (1988): Mat. Sci. and Eng., A105/106 p331-336

Goldstien D.E., Newbury D.E., Echlin P., Joy D.C.,Fiori C. and Lifshin E. (1981): "Scanning Electron Microscopy and X-Ray Microanalysis", p75,76,92,124

Gurland J. (1963): Trans. Amer. Soc. Metals, 50 p1063

Hack T.A. and Peters C.T. (1985): Paper HM5, Proc. 11th Plansee Seminar, Reutte, Austria

Human A.M., Northrop I.T., Luyckx S.B. and James M.N. (1992): J. of Hard Mat., 2 No3-4 p245-256

Jeffrey G.B. (1920): Proc. of the Roy. Soc. A, 221 p265-293

Larsen-Basse J. (1973): Powder Met., 16 No 31 p1-31

Larsen-Basse J. (1983): J. of Metals, p35-42

Laugier M.T. (1985 a): J. of Mat. Sci. Letters, 4 p263-264

Palmqvist S. (1963): Verkstäderna, 59 p187

Pennefather R.C. (1986): M.Sc. Thesis, UCT

Pennefather R.C., Hankey S.E., Hutchings R. and Ball A. (1988): Mat. Sci. and Eng., A105/106 (1988) p389-394

Rice J. R. and Johnson M.A. in Kanninen M.F., Adler W.F., Rosenfield A.R. and Jaffee R.I. (eds) (1970) "Inelastic behaviour of solids", Mc Graw-Hill, New York

Roebuck B. and Almond A.E. (1988): Intl Mat. Rev. 33 No2 p90

Roesler F. C. (1956): Proc. Phys. Soc. 69B p55

Rowcliff D.J., Jayaram V., Hibbs M.K. and Sinclair R. (1988): "Compressive deformation and fracture in WC materials", Materials Science and Engineering A 105/106 p299-303

Sharma N.K., Ward I.D., Fraser H.L. and Williams W.S. (1980): J. of the Amer. Ceram. Soc. 63 No 3-4 p194-196

Snell P.O. and Parnama E. (1973): Planseeber. Pulvermetall. 21 p17

Spiegler R., Schmauder S. and Exner H.E. (1992): J. of Hard Mat., 3 No2 p143-157

Swain M.V. and Hagan J.T. (1976): J. of Physics D: Applied Physics, 9 p2201-2214

Thouless M.D., Evans A.G., Ashby M.F. and Hutchinson J.W. (1987): Acta Metallurgica, 35 No6 p1333-1341

Tracey V.A. (1992): Refractory Metals and Hard Materials 11 p137-149

Tsai Y.M. and Kolsky H. (1967): J. of Mechanical Physics of Solids 15 p263-278

Warren R. (1978): Acta Metallurgica 26 p1759-1769

Wilshaw T.R. (1971): J. of Physics D: Applied Physics 4 p1567-1581